Progress In Electromagnetics Research, PIER 19, 1–48, 1998

TWO FUNDAMENTAL REPRESENTATIONS OF LOCALIZED PULSE SOLUTIONS TO THE SCALAR WAVE EQUATION *

I. Besieris and M. Abdel-Rahman

The Bradley Department of Electrical Engineering
Virginia Polytechnic Institute and State University
Blacksburg, VA 24061, USA

A. Shaarawi

Department of Engineering Physics and Mathematics
Faculty of Engineering, Cairo University, Giza, Egypt

A. Chatzipetros

Paging Group, Motorola
Boynton Beach, FL 33426, USA

* Dedicated to Professor Robert E. Collin on the occasion of his 70th birthday.

1. INTRODUCTION

The generation and propagation of carrier-free ultra-wideband pulses has attracted considerable attention in recent years [1–88, 93, 94]. This interest has been sustained by advancements in ultrafast acoustical, optical and electrical devices capable of generating and shaping very short pulsed wave fields [80]. These ultrashort pulses exhibit distinct advantages in their performance by comparison to conventional quasi-monochromatic signals. It has been shown, in particular, that such pulses have extended ranges of localization in the near-to-far field regions [cf. e.g., 18, 24]. In dispersive media, the shaping of their initial excitation can reduce significantly dispersive spreading [23, 78, 79, 85]. These properties, together with their uniform focused depth in the near field, render short pulsed wave fields very useful in applications involving high resolution imaging, nondestructive testing, secure signaling and interference-free communications.

In this paper, we are primarily interested in one class of ultra-wideband pulses that has become known as Localized Waves (LW). Examples of such pulsed fields include the Focus Wave Mode (FWM) derived by Brittingham [1], the Modified Power Spectrum (MPS) pulse deduced by Ziolkowski [18] and the X-wave introduced by Lu and Greenleaf [34]. Each LW pulse is a carrier-free, ultra-wideband wave field consisting of a highly focused central portion embedded in a sparse, low intensity background. Two scales, thus, characterize these pulsed wave fields: (i) an extremely small scale depicting the spatial extension and the temporal duration of the high intensity focused pulse; (ii) a larger scale specifying the size of the low intensity background field. This double trait causes LW pulses to behave in an extraordinary fashion when they propagate in free space and dispersive media, or scatter from objects. Another distinct feature of all LW pulses is an unusual coupling between their spatial and temporal spectral components. This coupling manifests itself as a time-dependent (dynamic) initial excitation on the source plane of the generated pulse; specifically, distinct segments of the source plane should be excited at different times using various time sequences. One factor determining the sequential order of the excitation of the various source elements is the spatio-temporal spectral coupling. The unusual structure of the frequency content of LW pulses causes the spectral depletion of the peaks of such pulsed wave fields to be entirely different from that of conventional quasi-monochromatic signals, or other broadband sig-

nals. Thorough investigations of the spectral depletion of LW pulses generated from finite-time dynamic apertures have been undertaken previously [61–64, 69–73, 85, 86]. A finite-time dynamic aperture is an artifice developed for studying the decay of propagating finite-energy LW pulses by time-limiting known closed-form infinite energy LW solutions. This provides a well-established scheme for shaping the spectral components of the initial field in a manner that it can control the decay rate of a LW pulse traveling away from its source plane. Such an approach is dependent on the *a priori* knowledge of exact closed-form LW solutions. It does not matter whether the known exact LW pulses have infinite energy, as long as the power content of the initial excitation on the source plane is always finite. In most cases, finite energy pulses can be generated by appropriately time-windowing the infinite energy excitation field.

The *bidirectional representation* of LW has been introduced in a previous publication by Besieris, Shaarawi and Ziolkowski [15] . It provides the most natural basis for deriving FWM-like solutions. The bidirectional representation utilizes the forward and backward characteristics of the wave equation as fundamental variables, and uses the corresponding spectral variables together with the transverse spectral components to synthesize exact LW solutions. This approach has been very successful as a comprehensive procedure for deriving closed-form FWM-like solutions. It turns out that the bidirectional superposition can easily be transformed into a Fourier one. This provides a great facility for transforming the spectral content of LW pulses derived using the bidirectional representation to the more conventional Fourier picture.

The main aim of this paper is to complement the bidirectional superposition with another representation based on the Lorentz boost variables of the wave equation; the latter are motivated from the Lorentz invariance of the wave equation. This allows us to boost stationary and separable elementary solutions in order to form propagating and nonseparable ones, for which the spatial and temporal quantities are combined together to compose the new boost variables. The main advantage of this new superposition is its capability of yielding X-wave type solutions. The latter have been shown to have the same basic properties as the FWM-like pulses, except that the form of their spatio-temporal spectral coupling is different [61, 86]. This causes the dynamic character of the aperture excitation field of an X-wave pulse

to be slightly different from that of a FWM field.

Traditionally, wave generation and propagation in linear media has been studied using Fourier analysis. The latter is one of the most powerful techniques developed to deal with linear systems. When Fourier analysis is applied to the scalar wave equation, one can work within the framework of either the Whittaker or the Weyl representation [cf., e.g., Ref. 92]. The former consists of a superposition of forward and backward traveling plane waves, while the latter is synthesized of converging and diverging waves together with the associated evanescent fields. Since a Fourier representation is a superposition of sinusoidal plane wave solutions, it is well suited to situations involving quasi-monochromatic signals. The bandwidth of the Fourier spectrum, in this case, is much smaller than the carrier frequency. As a consequence, a quasi-monochromatic wavetrain exists over a long time duration containing a large number of cycles of its significant frequency components. When one deals with ultra-wideband LW pulses, on the other hand, the axial length of the highly focused central portion of the pulse equals the shortest wavelength contributing to its Fourier spectrum. It is more appropriate, then, to synthesize LW pulses using other localized basis functions. Ziolkowski, who constructed the MPS pulse as a superposition of FWM solutions, made the first attempt towards such a direction [18]. Along the same vein, the realization that FWM-like solutions involved the natural characteristic variables $(z - ct)$ and $(z + ct)$ of the wave equation led to the development of the bidirectional representation. That effort was undertaken in order to serve two specific goals: (i) to provide a more general framework for deriving FWM-like solutions; (ii) to devise a scheme that could easily transform the deduced spectral information into the Fourier picture. The latter is a crucial step because even if a Fourier superposition is not the most natural representation of LW solutions, the information included in their Fourier spectrum is necessary for any attempts to construct physical sources. The practical limitations and characteristics of the devices used to manufacture a real source are ultimately formulated in terms of Fourier terminology. In this work, we extend our previous attempt to introduce new representations well suited to the construction of exact LW solutions, and to describe how to relate these representations to the Fourier picture.

The plan of this work is to start by reviewing the fundamental aspects of the bidirectional representation. This is done in Sec. 2,

where we demonstrate that the bidirectional representation can be transformed into a new superposition involving a product of plane waves traveling along the subluminal and superluminal boost variables. We show that the former representation is more suitable for deriving FWM-like pulses, while the latter is more appropriate for dealing with X-wave type solutions. Moreover, we demonstrate how the same finite-energy LW pulses can be deduced using both representations. The physical origin of the boost representation is described in Sec. 3. It is shown that the boost representation follows naturally from the invariance of the scalar wave equation under Lorentz transformations. These invariance properties are illustrated by using the Lorentz boost to transform elementary solutions, given in a specific frame of reference, into subluminally or superluminally propagating LW pulses. The power and flexibility provided by the two fundamental representations of LW solutions are used in Sec. 4 to deduce new closed-form solutions representing finite-energy LW pulses. In Sec. 5, we comment on an interesting behavior of the excitation wave fields acting on the source planes of the LW pulses. Concluding remarks to this work are made in Sec. 6.

2. TWO FUNDAMENTAL SUPERPOSITIONS

The homogeneous scalar wave equation

$$\left(\nabla^2 - \frac{1}{c^2}\frac{\partial^2}{\partial t^2}\right)\Psi(\vec{r},t) = 0 \tag{2.1}$$

has two fundamental properties: (i) it is invariant under Lorentz boosts; (ii) pulsed solutions traveling along the z-axis have two natural characteristic variables, $\zeta = z - ct$ and $\eta = z + ct$. Nonseparable localized solutions to the wave equation can be derived from superpositions based on these two natural attributes. The bidirectional superposition is associated with the second property. Since its introduction in 1989, it has been used extensively to derive different kinds of localized waves. Furthermore, it has proved very useful in deducing unusual spectra that are not easily motivated from a Fourier perspective. Due to its simple form, the bidirectional representation can be transformed in a straightforward manner into a Fourier superposition. The ability to move from one picture to the other provides a great advantage. It permits one to derive unusual LW solutions and subsequently deduce

the corresponding Fourier spectra. The latter can then be used to identify various attributes characterizing the excitation of LW sources. In this section, we review briefly some of the properties of the bidirectional superposition and then derive a new representation based on superluminal or subluminal boost variables.

We start with the azimuthally symmetric bidirectional representation of a solution to the scalar wave equation:

$$\Psi(\rho,\zeta,\eta)=\int_0^\infty d\alpha\int_0^\infty d\beta\int_0^\infty d\chi\chi J_0(\chi\rho)e^{-i\alpha\zeta}e^{+i\beta\eta}\Phi(\chi,\alpha,\beta)\delta(\alpha\beta-\chi^2/4). \tag{2.2}$$

This superposition can be transformed to the Fourier picture by realizing that $\alpha=((\omega/c)+k_z)/2$ and $\beta=((\omega/c)-k_z)/2$. This procedure has been described in detail in Ref. 15 and has subsequently been used to derive LW solutions directly from Fourier superpositions. Without loss of generality, we carry out the integration over α to obtain

$$\Psi(\rho,\zeta,\eta)=\int_0^\infty d\beta\int_0^\infty d\chi\chi J_0(\chi\rho)e^{-i(\chi^2/4\beta)\zeta}e^{+i\beta\eta}\tilde{\Phi}(\chi,\beta), \tag{2.3}$$

where $\tilde{\Phi}(\chi,\beta)=\Phi(\chi,\alpha,\beta)/\beta$, with $\alpha=\chi^2/4\beta$. Some of the well-known LW exact solutions to the scalar wave equation are readily derivable using the superposition (2.3). For example, the singular spectrum

$$\tilde{\Phi}(\chi,\beta)=\frac{1}{2\beta}e^{-(\chi^2/4\beta)a_1}\delta(\beta-\beta'),\quad a_1>0, \tag{2.4}$$

yields the FWM solution [5]

$$\Psi_{FWM}(\rho,z,t)=\frac{1}{a_1+i\zeta}e^{-\beta'\rho^2/(a_1+i\zeta)}e^{i\beta'\eta}. \tag{2.5}$$

Similarly, the MPS pulse is derived using the spectrum

$$\tilde{\Phi}(\chi,\beta)=\begin{cases}\dfrac{p}{2\beta\Gamma(q)}(p\beta-b)^{q-1}e^{-\chi^2a_1/4\beta}e^{-a_2(p\beta-b)} & \text{for } \beta\geq b/p\\ 0 & \text{for } b/p>\beta>0,\end{cases} \tag{2.6}$$

where $a_2 > 0$. For $q = 1$, the superposition (2.3) results in the finite energy LW pulse

$$\Psi_{MPS}(\rho, z, t) = \frac{1}{(a_1 + i\zeta)} \frac{1}{[(\rho^2/(a_1 + i\zeta)) - i\eta + pa_2]} \times e^{-b\rho^2/p(a_1+i\zeta)} e^{ib\eta/p}. \tag{2.7}$$

This solution was originally derived by Ziolkowski [18] as a Laplace-type superposition of infinite energy FWM solutions, viz.,

$$\Psi(\vec{r}, t) = \int_0^\infty d\beta' F(\beta') \Psi_{FWM}(\rho, z, t; \beta'). \tag{2.8}$$

The main difference between the two spectra given in (2.4) and (2.6), respectively, is that the former includes a Dirac delta function and the latter does not. A Laplace-type integration of weighted FWM solutions over the parameter β' introduces a continuous spread in the values of β around β'. Consequently, the singular distribution $\delta(\beta - \beta')$ is transformed through the integration (2.8) into a continuous distribution over a range of β values. This is a recurring theme encountered whenever a finite energy solution is derived. Notice, also, that singular spectra analogous to (2.4) yield LW solutions whose envelopes are functions only of ζ. Obviously, an envelope depending only on ζ propagates in the positive z-direction without spreading out. However, the total energy content of such LW pulses is infinite. Once we depart from delta distributions in the spectrum $\tilde{\Phi}(\chi, \beta)$, and the parameter β is spread over a range of values, we obtain finite energy LW solutions. The resulting LW solutions [e.g., the MPS pulse given in Eq. (2.7)] have envelopes that depend on both characteristics ζ and η. This mixing of the two characteristic variables causes a finite energy LW pulse to decay as it propagates beyond a certain focused range along the z-axis.

The two solutions given in Eqs. (2.5) and (2.7) have been studied extensively and there is no specific reason to elaborate on their properties except to compare them to other LW solutions deduced in later sections. For such a purpose we plot, in Fig. (1), the FWM pulse for $a_1 = 0.0001$ m and $\beta' = 1$. The negative ρ values in the figure should be understood to be the image of the positive ones along any arbitrary transverse direction. The FWM pulse periodically acquires

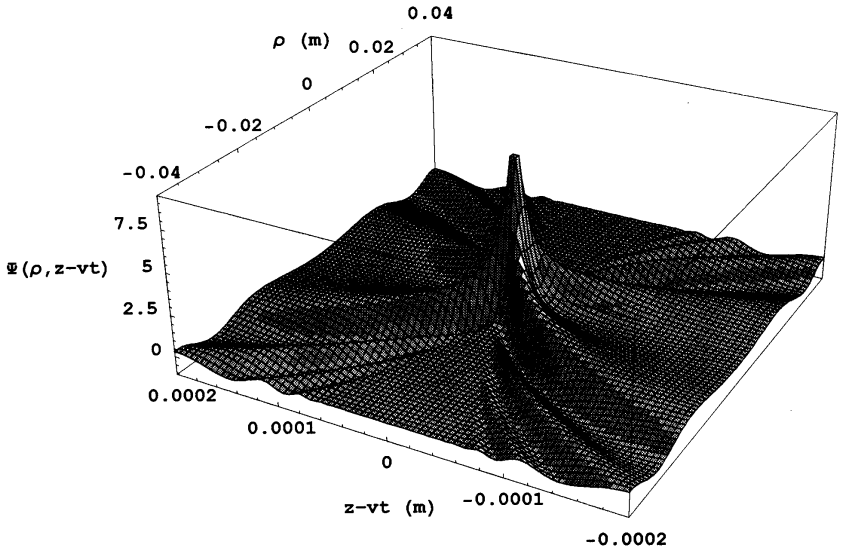

Figure 1. Surface plot of the real part of the Focus Wave Mode (FWM) pulse with parameters $a_1 = 10^{-4}$ m and $\beta' = 1$.

the form shown in the figure at distances $z = n\pi/\beta$, where n is an integer. The radius of the focused part of the FWM field is of order $\sqrt{a_1/\beta}$. The finite energy MPS pulse [cf. Eq. (2.7)] initially resembles the FWM. The radius of its focused region is equal to $\sqrt{pa_1/b}$ and it starts decaying as $(1/z)$ for $z > (pa_2/2)$.

To demonstrate the facility by which other solutions analogous to those given in (2.5) and (2.7) can be deduced, consider the following bidirectional spectrum:

$$\tilde{\Phi}(\chi, \beta) = \frac{1}{2\beta} e^{-\chi^2 a_1/\beta} J_0(\chi a) \delta(\beta - \beta'), \quad a_1 > 0. \tag{2.9}$$

Because of the singular spectral dependence on β', the superposition (2.3) gives the infinite energy Focus Splash Mode (FSM) solution

$$\Psi_{FSM}(\rho, z, t) = \frac{1}{a_1 + i\zeta} e^{-\beta(a^2+\rho^2)/(a_1+i\zeta)} I_0\Big(2a\beta\rho/(a_1 + i\zeta)\Big) e^{i\beta\eta}. \tag{2.10}$$

In a superposition over $\Psi_{FSM}(\rho, z, t)$ analogous to Eq. (2.8), the substitution of the spectrum $F(\beta) = \exp(-\beta a_2)$ yields the finite energy

Modified Splash (MS) pulse

$$\Psi_{MS}(\rho,z,t)=\frac{1}{(a_1+i\zeta)}\left\{\left[\frac{a^2+\rho^2}{(a_1+i\zeta)}+(a_2-i\eta)\right]^2-\frac{4\rho^2a^2}{(a_1+i\zeta)^2}\right\}^{-\frac{1}{2}}. \tag{2.11}$$

In the limit $a\to 0$, the above expression reduces to the ordinary splash pulse, of order $q=1$, introduced previously [4, 21]. The MS pulse given in Eq. (2.11) is plotted for the parameter values $a_1=10^{-4}$ m, $a_1=10^{-3}$ m and $a_2=1000$ m. The surface plots shown in Figs. (2.a–d) correspond to the distances $ct=0$, 500, 1000 and 2000 m. These figures show that the MS spreads out beyond a certain range. The resemblance between the shape of the spreading MS and MPS pulses should be noted [e.g., compare with plots in Ref. 18]. However, unlike the MPS and FWM fields, the focused portion of the MS pulse decays monotonically and does not exhibit the oscillatory behavior along the direction of propagation characterizing the former two pulses. The parameters included in the solution affect the shape of the propagating pulse. Specifically, smaller a_1 values result in shorter pulses that have narrower waists. On the other hand, the parameter a_2 determines the dispersion-free range of the propagating MS pulse.

The examples considered so far in this section demonstrate the great facility provided by the bidirectional representation in deriving LW solutions. In previous work [61–64, 69–73, 85–87], schemes for generating good approximations to LW solutions were developed and the spectral depletion of the launched LW pulses was studied in detail. The parameters included in the exact solutions affect the various attributes of the initial excitation of a LW aperture and, consequently, control the decay rates of the propagating pulses. In an effort to characterize the decay behavior of LW pulses, it has been established that the spectral depletion of LW pulses differs entirely from that of quasi-monochromatic as well as other broadband signals. When compared to other pulsed beams, LW pulses exhibit an extended range of localization in the near-to-far field regime. However, the behavior of different LW pulses may vary over their ranges of localization. As a consequence, being able to derive new exact solutions is a vital tool in the study of such pulsed wave fields. Basically, one may search for infinite energy solutions characterized by a singular bidirectional spectrum. Large numbers of closed-form expressions for these infinite energy pulses can be derived easily from the bidirectional representation because of the Dirac delta

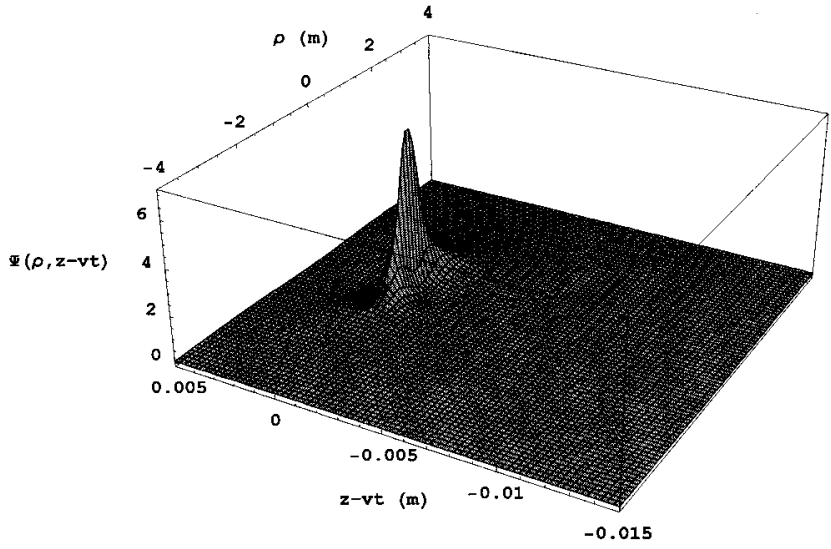

(a) $\nu t = 0$ m.

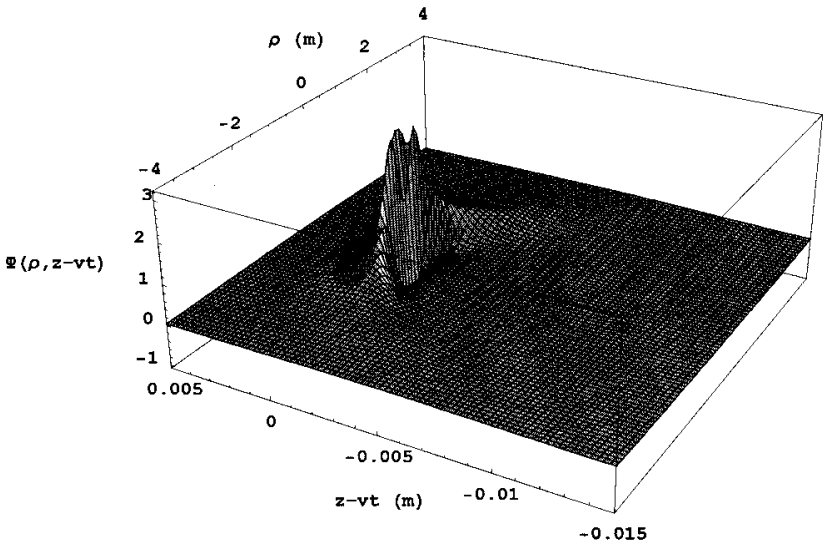

(b) $\nu t = 500$ m.

Figure 2(a-b). Surface plot of the real part of the Modified Splash (MS) pulse with parameters $a_1 = 10^{-4}$ m, $a = 10^{-3}$ and $a_2 = 10^{3}$ m.

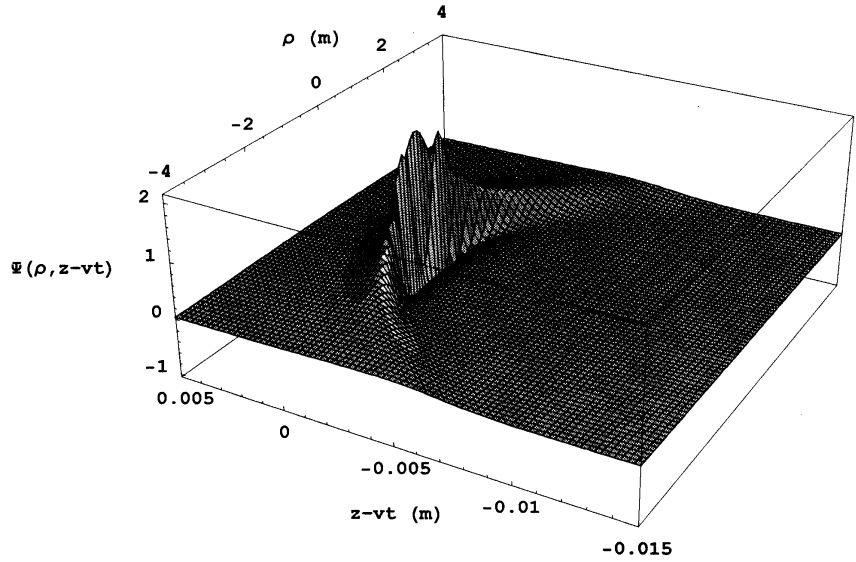

(c) $\nu t = 1000$ m.

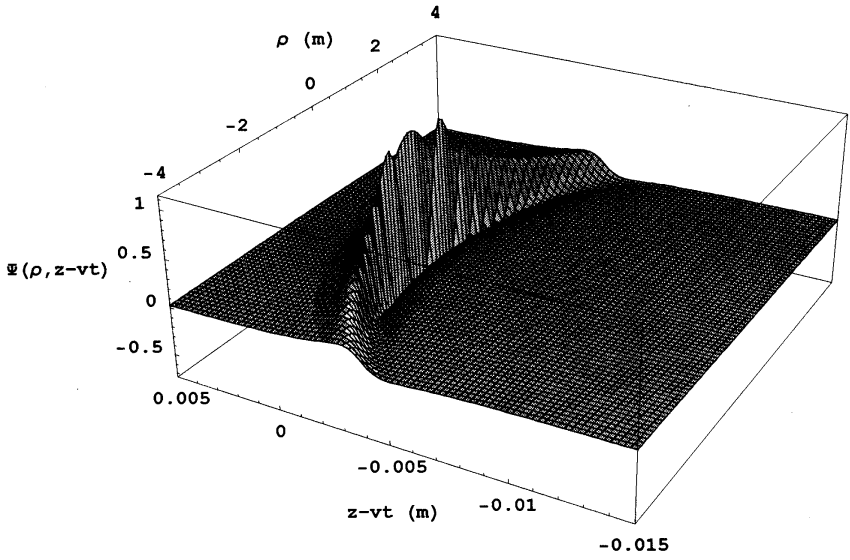

(d) $\nu t = 2000$ m.

Figure 2(c-d). Surface plot of the real part of the Modified Splash (MS) pulse with parameters $a_1 = 10^{-4}$ m, $a = 10^{-3}$ and $a_2 = 10^{3}$ m.

functions included in their spectra. The presence of the Dirac delta functions reduces the number of multiple integrals to be evaluated. These simple closed-form expressions help in understanding the general features of the deduced LW solutions. Finite energy pulses can then be derived simply by smoothing the singular spectrum, thus allowing the argument of the delta function to acquire a distribution over a finite range of values. The smoothing of the singular spectrum adds an extra integration and, in most cases, closed-form expressions for finite energy solutions cannot be derived. Guided, however, by our knowledge of the behavior of infinite energy pulses, numerical investigations of finite energy solutions can be carried out. The point we wish to emphasize is that deriving closed-form expressions is vital to any thorough investigation of LW pulses. No wonder most investigations have been centered on exact LW solutions, e.g., FWM, MPS and X-wave pulses. In this work, our main objective is to demonstrate how to deduce closed-form expressions of various types of LW solutions. Furthermore, we would like to show how seemingly disparate types of pulses might be linked together.

The few examples discussed so far in this section are variants of the source-free FWM pulse. There is another type of a LW solution, namely the X-wave, that has been developing independently [34–36, 47, 60, 65–67, 74–76, 82–84, 94]. The X-wave has a closed-form expression that appears to be very different from that of the FWM pulse. However, the generation and propagation characteristics of these wavefields show great similarities [61, 86, 87]. Both are tightly focused, high intensity, pulsed wavefields embedded in an extended background of a much lower magnitude. They have extended ranges of localization in the near-to-far field limit and are generated by dynamic apertures for which the size of the active area of the initial excitation is time dependent. Furthermore, it has been shown [61, 86, 87] that the X-wave and the FWM pulses have very similar spectral structures. They only differ in the way their respective spatial and temporal frequency components are coupled together. The coupling of the spatial and temporal spectral components is an essential feature characterizing all LW solutions. Based on these observations, we would like to raise the following question: How can two pulses that have so much in common be related to each other? Apparently, it is not very clear how to derive the X- wave solution from a bidirectional superposition.

In the sequel, we shall demonstrate that the bidirectional representation is linked to a new representation based on subluminal or superluminal boost variables. First we introduce the subluminal variables $\bar{\tau} = -\bar{\gamma}(\nu/c)(z - (c^2/\nu)t)$ and $\bar{\sigma} = \bar{\gamma}(z - \nu t)$, where $\bar{\gamma} = (1 - (\nu/c)^2)^{-1/2}$ for $(\nu/c) < 1$. These new variables are just the subluminal Lorentz boosts of z and t. They are natural variables of the wave equation because the latter is invariant under a Lorentz transformation. Using these new variables, the characteristic variables are rewritten as

$$\zeta = z - ct = \bar{\gamma}\,(1 - (\nu/c))\,(\bar{\sigma} - \bar{\tau})$$

and

$$\eta = z + ct = \bar{\gamma}\,(1 + (\nu/c))\,(\bar{\sigma} + \bar{\tau}). \tag{2.12}$$

The relation between the characteristic variables and the subluminal boost variables transforms the bidirectional representation (2.2) into the superposition

$$\Psi(\rho,\sigma,\tau) = \int_{-\infty}^{+\infty} d\kappa \int_{0}^{\infty} d\lambda \int_{0}^{\infty} d\chi\chi J_0(\chi\rho) e^{+i\kappa\bar{\sigma}} e^{+i\lambda\bar{\tau}} \cdot \Phi(\chi,\kappa,\lambda)\delta(\lambda^2 - \kappa^2 - \chi^2), \tag{2.13}$$

where

$$\kappa = \beta\bar{\gamma}(1 + (\nu/c)) - \alpha\bar{\gamma}(1 - (\nu/c))$$

and

$$\lambda = \beta\bar{\gamma}(1 + (\nu/c)) + \alpha\bar{\gamma}(1 - (\nu/c)) \tag{2.14}$$

In Eq. (2.13), the lower bound on λ is 0 and not $-\infty$ by virtue of Eqs. (2.2) and (2.14). It is clear that for α and β positive [see the limits in Eq. (2.2)], λ should acquire only positive values. The integration over κ in Eq. (2.13) yields the subluminal boost representation

$$\Psi(\rho,\sigma,\tau) = \int_{-\infty}^{+\infty} d\lambda \int_{0}^{\infty} d\chi\chi J_0(\chi\rho) e^{+i\sqrt{\lambda^2-\chi^2}\bar{\sigma}} e^{+i\lambda\bar{\tau}} \tilde{\Phi}(\chi,\lambda). \tag{2.15}$$

The limits of the integration over λ change to $-\infty$ to $+\infty$ to accommodate the negative and positive roots of the Dirac delta function. For

$\chi^2 > \lambda^2$, the integration must be analytically continued using a suitable complex contour integration. The above superposition resembles the Weyl representation of solutions to the scalar wave equation, with the variables z and t replaced by the subluminal boost variables $\bar{\sigma}$ and $\bar{\tau}$, respectively. Similarly, the superluminal boost variables are introduced as $\sigma = \gamma(\nu/c)(z - (c^2/\nu)t)$ and $\tau = -\gamma(z - \nu t)$, where $\gamma = ((\nu/c)^2 - 1)^{1/2}$ for $(\nu/c) > 1$. The conventional characteristic variables are related to σ and τ as follows:

$$\zeta = z - ct = \gamma\left((\nu/c) - 1\right)(\sigma - \tau)$$

and

$$\eta = z + ct = \gamma\left((\nu/c) + 1\right)(\sigma - \tau) \tag{2.16}$$

Introducing the relations given in (2.16) into (2.2), we obtain

$$\Psi(\rho,\sigma,\tau) = \int_{-\infty}^{+\infty} d\kappa \int_{0}^{\infty} d\lambda \int_{0}^{\infty} d\chi\chi J_0(\chi\rho) e^{+i\kappa\sigma} e^{+i\lambda\tau} \cdot \Phi(\chi,\kappa,\lambda)\delta(\lambda^2 - \kappa^2 - \chi^2), \tag{2.17}$$

where

$$\kappa = \beta\gamma\left((\nu/c) + 1\right) - \alpha\gamma\left((\nu/c) - 1\right)$$

and

$$\lambda = \beta\gamma\left((\nu/c) + 1\right) + \alpha\gamma\left((\nu/c) - 1\right) \tag{2.18}$$

The integration over λ gives the superluminal representation

$$\Psi(\rho,\sigma,\tau) = \int_{-\infty}^{+\infty} d\kappa \int_{0}^{\infty} d\chi\chi J_0(\chi\rho) e^{+i\kappa\sigma} e^{+i\sqrt{\kappa^2+\chi^2}\tau} \tilde{\Phi}(\chi,\kappa). \tag{2.19}$$

It should be noted that this superposition resembles the Whittaker representation of solutions to the scalar wave equation, except that the variables z and t are replaced by the boost variables σ and τ, respectively. The superluminal representation (2.19) is a superposition of a product of two plane waves, one moving along the positive z-direction with speed $\nu > c$ and the other traveling in the same direction at a speed $(c^2/\nu) < c$. Although these two plane waves appear

to be unidirectional, the superposition (2.19) consists generally of forward and backward traveling components. The same property is more apparent in the bidirectional representation. In both cases, one should be careful to isolate the backward traveling components in order to be able to generate a completely causal forward traveling wavefield. In some solutions, like the X-wave, the traveling pulse consists solely of forward propagating plane waves.

Superpositions leading to X-wave-type solutions follow naturally from the representation given in Eq. (2.19) by choosing the singular spectrum

$$\tilde{\Phi}(\chi, \kappa) = \tilde{\Phi}_n(\chi)\delta(\kappa). \tag{2.20}$$

The substitution of the relation (2.20) reduces Eq. (2.19) to the familiar X-wave superposition

$$\Phi(\rho, z, t) = \int_0^\infty d\chi \chi J_0(\chi\rho) e^{-i\gamma\chi(z-\nu t)} \tilde{\Phi}_n(\chi). \tag{2.21}$$

The specific spectrum

$$\tilde{\Phi}_0(\chi) = e^{-\chi a_1}/\chi, \quad a_1 > 0, \tag{2.22}$$

yields the conventional zeroth order X-wave [cf. Ref. 34]

$$\Phi_{XW}^{(0)}(\rho, z, t) = \frac{1}{\left(\rho^2 + \left(a_1 + i\gamma(z - \nu t)\right)^2\right)^{1/2}}. \tag{2.23}$$

Higher order X-wave solutions can be derived simply choosing the spectrum $\tilde{\Phi}_n(\chi) = \chi^n e^{-\chi a_1}$, $n > 0$. In Fig. (3), we provide a 3-D surface plot of the X-wave for the parameter values $a_1 = 0.0001$ m and $(\nu/c) = 1.0001$. One should note that away from the central focused portion the background field branches out to acquire the distinct shape of the letter X.

Since a simple change of variables transforms the bidirectional representation into the Lorentz boost variable representation, one can show that the X-wave solution may be directly inferred from the bidirectional representation. The transformation of the α and β variables into $\alpha\chi$ and $\beta\chi$, respectively, modifies the bidirectional representation (2.2) into the following form [61]:

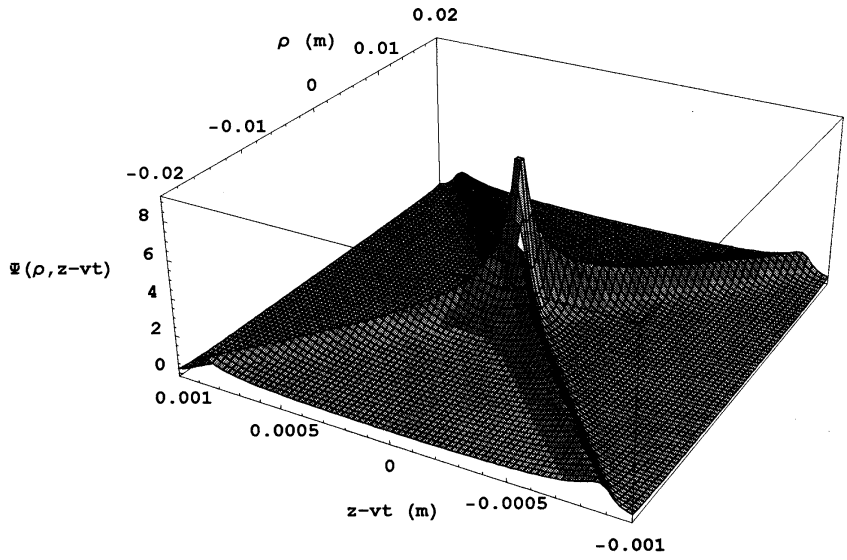

Figure 3. Surface plot of the real part of the X-wave pulse with parameters $a_1 = 10^{-4}$ m and $\nu/c = 1.0001$.

$$\Psi(\rho,\zeta,\eta) = \int_0^\infty d\alpha \int_0^\infty d\beta \int_0^\infty d\chi\chi J_0(\chi\rho) e^{-i\alpha\chi\zeta} e^{+i\beta\chi\eta}.$$

$$\Phi(\chi,\alpha,\beta)\delta(\alpha\beta - 1/4). \qquad (2.24)$$

The integration over α gives

$$\Psi(\rho,\zeta,\eta) = \int_0^\infty d\beta \int_0^\infty d\chi\chi J_0(\chi\rho) e^{-i(\chi/4\beta)\zeta} e^{+i\beta\chi\eta} \tilde{\Phi}(\chi,\beta). \qquad (2.25)$$

A spectrum analogous to the one given in equation (2.22), namely $\tilde{\Phi}(\chi,\beta) = \delta(\beta-\beta')e^{-\chi a_1}/\chi$, yields the X-wave solution [cf. Eq. (2.23)], with $(\nu/c) = (1+4\beta'^2)/(1-4\beta'^2)$ and $\gamma = (1-4\beta'^2)/4\beta'$. This is a remarkable result because it demonstrates that a specific choice of a bidirectional spectrum leads to an X-wave solution traveling along a boost variable instead of the characteristic variables used in Eq. (2.25).

The same applies to a Whittaker representation consisting of plane waves characterized by the spectral Fourier variables ω, χ, and k_z. With a proper choice of spectra, one can use the Whittaker superposition to derive any of the known LW solutions. The important point is to use the most natural representation and to be able to transform the results from one picture to another. For example, the only possible way to get to the Fourier spectrum of the MPS pulse is through a transformation of its bidirectional spectrum into a Fourier one.

In closing this section, we shall show by means of a specific example how to synthesize finite energy LW pulses as superpositions of infinite energy X-wave type solutions. Towards this goal, we substitute the spectrum

$$\tilde{\Phi}(\chi,\beta)=\sqrt{\frac{4\chi}{\pi\beta^3}}e^{-\chi a_1/\beta}e^{-\beta\chi a_2} \tag{2.26}$$

into the modified bidirectional representation (2.25). Next, we introduce the new variable $\bar{\beta}=\sqrt{\beta}$ and use the relation (3.472.3) in Gradshteyn and Ryzhik [90] to carry out the integration over $\bar{\beta}$:

$$\Psi(\rho,\zeta,\eta)=\int_0^\infty d\chi J_0(\chi\rho)\frac{1}{\sqrt{a_1+i\zeta}}e^{-\chi\sqrt{(a_1+i\zeta)(a_2-i\eta)}}. \tag{2.27}$$

The integration over χ is carried out using the identity (6.611.1) in Ref. 90 to obtain

$$\Psi_{SP}(\rho,z,t)=\frac{1}{\sqrt{a_1+i\zeta}}\left\{\rho^2+(a_1+i\zeta)(a_2-i\eta)\right\}^{-1/2}. \tag{2.28}$$

This is the splash pulse corresponding to $q=1/2$. When the spectrum (2.26) is substituted in Eq. (2.25), but the order of integration is reversed, the integration over χ can be carried out using formula (6.62) in Ref. 90, yielding

$$\Psi_{SP}(\rho,z,t)=\int_0^\infty d\bar{\beta}\frac{1}{\bar{\beta}^2}\Psi_{PXW}(\rho,z-\nu(\bar{\beta})t;\bar{\beta}). \tag{2.29}$$

This shows that the splash pulse (2.28) can be derived as a superposition of Legendre X-wave defined as

$$\Psi_{PXW}(\rho,z,t) = \frac{1}{\left\{\left(\Lambda(\bar{\beta})+i\gamma(\bar{\beta})(z-\nu(\bar{\beta})t)\right)^2+\rho^2\right\}^{3/4}} \cdot P^0_{1/2}\left\{\frac{\left(\Lambda(\bar{\beta})+i\gamma(\bar{\beta})(z-\nu(\bar{\beta})t)\right)}{\sqrt{\left(\Lambda(\bar{\beta})+i\gamma(\bar{\beta})(z-\nu(\bar{\beta})t)\right)^2+\rho^2}}\right\} \quad (2.30)$$

where $P^0_{1/2}$ is an associated Legendre function of the first kind and $\Lambda(\bar{\beta}) = (a_1/4\bar{\beta}^2) + a_2\bar{\beta}$. The pulsed solution given in Eq. (2.30) is nondispersive and its center travels at the superluminal speed $\nu(\bar{\beta}) = c(1+4\bar{\beta}^4)/(1-4\bar{\beta}^4)$ with $\gamma(\bar{\beta}) = (1-4\bar{\beta}^4)/4\bar{\beta}^2$.

The analysis presented in this section shows that apparently two disparate types of solutions exhibit fundamental congruencies. There are no fundamental differences between the FWM-type and the X-wave-type LW solutions. It appears, however, that the most natural representation of the former is in terms of the characteristic variables η and ζ, while it is more natural to utilize the superluminal boost variables σ and τ in the latter case. Finite energy LW solutions can be derived using either of the two representations. Before applying the procedure derived here to obtain new finite energy LW solutions, we would like to elaborate on the origin of the boost variables. In the following section, we will utilize the Lorentz invariance of the wave equation to generate new LW solutions.

3. THE INVARIANCE OF SOLUTIONS TO THE WAVE EQUATION

The boost variables entering into the subluminal and superluminal fundamental representations given in Eqs. (2.15) and (2.19), respectively, ensue from the invariance of the wave equation under generalized Lorentz transformations, viz.,

$$ct \to \bar{\tau} = \bar{\gamma}(ct-(\nu/c)z), \quad z \to \bar{\sigma} = \bar{\gamma}(z-\nu t),$$
$$y \to y \quad \text{and} \quad x \to x \quad \text{for} \quad \nu < c. \quad (3.1.a)$$

and

$$ct \to \tau = \gamma(\nu t - z), \quad z \to \sigma = \gamma((\nu/c)z - ct),$$
$$y \to y \quad \text{and} \quad x \to x \quad \text{for} \quad \nu > c. \tag{3.1.b}$$

The knowledge of this invariance property facilitates the derivation of various LW waves.

3.1 General Boost Representations

Consider the Fourier-Bessel transform of the scalar wave equation, viz.,

$$\left(\frac{\partial^2}{\partial z^2} - \frac{1}{c^2}\frac{\partial^2}{\partial t^2} - \chi^2\right)\tilde{\psi}(\chi, z, t) = 0, \tag{3.2}$$

which is an $(1+1)$ Klein-Gordon equation. This equation has elementary solutions of the form

$$\tilde{\psi}_e(\chi, z, t) = \Phi(\chi, \kappa, \lambda)e^{i\kappa z}e^{i\lambda ct}, \tag{3.3}$$

as long as the condition $\lambda^2 - \kappa^2 - \chi^2 = 0$ is satisfied. From the Lorentz invariance of the scalar wave equation, we know that boosted solutions still satisfy the same equation. Consequently, using either of the transformations (3.1.a) or (3.1.b) to boost $\tilde{\psi}_e(\chi, z, t)$ given in Eq. (3.3) yields a new elementary solution to Eq. (3.2). The evaluation of the inverse Hankel transform of the boosted elementary function, followed by a superposition over all values of κ and λ, yields the general subluminal and superluminal representations given in Eqs. (2.15) and (2.19), respectively. A large number of new LW solutions may be derived following this path. In the following, we will present a few examples demonstrating the facility provided by the invariance principle in generating exact LW solutions.

3.2 X-Wave Superpositions Arising from Boosts of Solutions to the 2-D Wave Equation

Consider solutions to Eq. (3.2) that are independent of z; the latter obey the $(1+2)$ transformed wave equation

$$\left(-\frac{1}{c^2}\frac{\partial^2}{\partial t^2} - \chi^2\right)\tilde{\psi}(\chi, t) = 0. \tag{3.4}$$

An elementary solution to Eq. (3.4) is $\tilde{\psi}_e(\chi, t) = \tilde{\Phi}(\chi) \exp(i\chi ct)$. Applying the inverse Hankel transform to this solution, we obtain

$$\psi(\rho, t) = \int_0^\infty d\chi \chi J_0(\chi\rho) e^{i\chi ct} \tilde{\Phi}(\chi). \tag{3.5}$$

A superluminal boost $ct \to \gamma(\nu t - z)$ yields the X-wave type superposition; specifically,

$$\Psi(\rho, z, t) = \int_0^\infty d\chi \chi J_0(\chi\rho) e^{-i\gamma\chi(z-\nu t)} \tilde{\Phi}(\chi).$$

The subluminal transformation (3.1.a) results in a similar expression representing a pulse traveling with $(c^2/\nu) > c$. Different choices of the spectrum $\tilde{\Phi}(\chi)$ give various types of infinite energy X-wave type solutions. Examples of these exist in the literature and have been discussed briefly in Sec. 2. In closing, we would like to point out that our work in this subsection provides a fundamental explanation for the procedure followed recently by Lu, Zou, and Greenleaf [65] in deriving a superluminal X-wave superposition.

3.3 Localized Waves Arising from Boosts of Solutions to the 3-D Laplace Equation

Consider, next, solutions to Eq. (3.2) that are independent of t. In this case, we have the reduced equation

$$\left(\frac{\partial^2}{\partial z^2} - \chi^2 \right) \tilde{\psi}(\chi, z) = 0. \tag{3.6}$$

An elementary solution to this equation is given by $\tilde{\psi}_e(\chi, z) = \tilde{\Phi}(\chi) \exp(\pm\chi z)$ for $\mp z > 0$. The inverse Hankel transformation gives the following solution to the 3-D Laplace equation:

$$\psi(\rho, t) = \int_0^\infty d\chi \chi J_0(\chi\rho) e^{\pm\chi z} \tilde{\Phi}(\chi), \quad \text{for } \mp z > 0. \tag{3.7}$$

The subluminal boost $z \to \bar{\gamma}(z - \nu t)$ yields a solution to the scalar wave equation in the form of a Laplace-type superposition; specifically,

$$\Psi(\rho, z, t) = \int_0^\infty d\chi \chi J_0(\chi\rho) e^{\pm\bar{\gamma}\chi(z-\nu t)} \tilde{\Phi}(\chi), \quad \text{for} \quad \mp(z - \nu t) > 0. \tag{3.8}$$

A large number of closed-form solutions may be derived using a Laplace transform table. As an example, we use the spectrum

$$\tilde{\Phi}(\chi) = \frac{1}{\chi} e^{-\chi(a_1 + i a_2)} \tag{3.9}$$

to obtain

$$\Psi(\rho, z, t) = \int_0^\infty d\chi J_0(\chi\rho) e^{-\chi(a_1 + i a_2 \pm \bar{\gamma}(\nu t - z))}. \tag{3.10}$$

The integration over χ gives the following solution:

$$\Psi(\rho, z, t) = \begin{cases} \dfrac{1}{\left(\rho^2 + (a_1 + i a_2 + \bar{\gamma}(\nu t - z))^2\right)^{1/2}}, & \text{for } (\nu t - z) > 0 \\ \dfrac{1}{\left(\rho^2 + (a_1 + i a_2 + \bar{\gamma}(z - \nu t))^2\right)^{1/2}}, & \text{for } (z - \nu t) > 0 \end{cases} \tag{3.11}$$

This solution is valid under the following restriction. Eq. (3.10) requires $\mathrm{Re}\{a\} > 0$, with $a = a_1 + i a_2 \pm \gamma(\nu t - z)$. Then, in Eq. (3.11), the value of the square root should be taken that obeys the constraint $|a + (a^2 + \rho^2)^{1/2}| > \rho$. Plots of this solution are shown in Fig. (4) for different values of the parameters a_1, a_2 and (ν/c). The main characteristic of this field is that the peak of the pulse (3.11) does not occur on the axis $(\rho = 0)$. Instead, the part of the propagating field acquiring higher intensities forms a cylindrical ring. The transverse radius of this ring is dependent on a_2, while its length along the direction of propagation increases as (ν/c) becomes smaller. These effects are illustrated in Figs. (4.a–c). Comparing Figs. (4.a) and (4.b) we note that for $(\nu/c) = 0.9$ the pulse is much longer than for $(\nu/c) = 0.9999$. Furthermore, the annular ring thins out in the transverse direction, as it becomes longer. In Fig. (4.c), it is shown that the radial position of the annular ring becomes larger than in Fig. (4.a) when a_2 is increased to the value 2.5×10^{-2} m.

The Hankel representation given in Eq. (3.7) is a solution to the 3-D Laplace equation. This means that boosting other solutions to the Laplace equation leads to functions satisfying the 3-D scalar wave

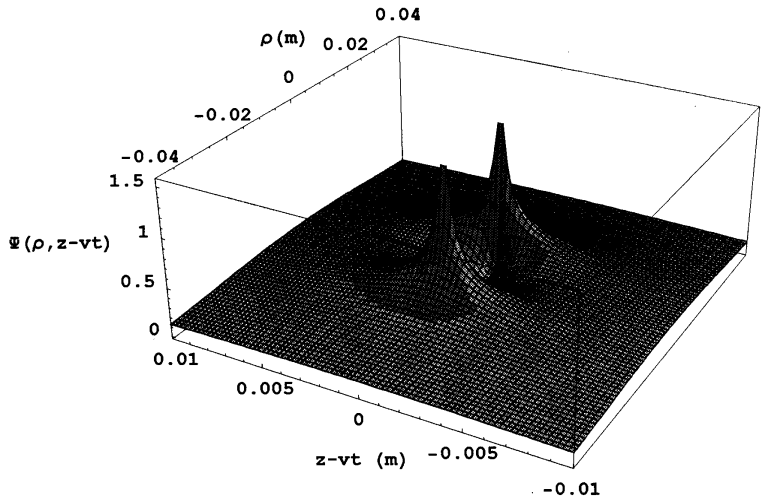

(a) $a_1 = 10^{-5}$ m, $a_2 = 10^{-2}$ m, $\nu/c = 0.9999$.

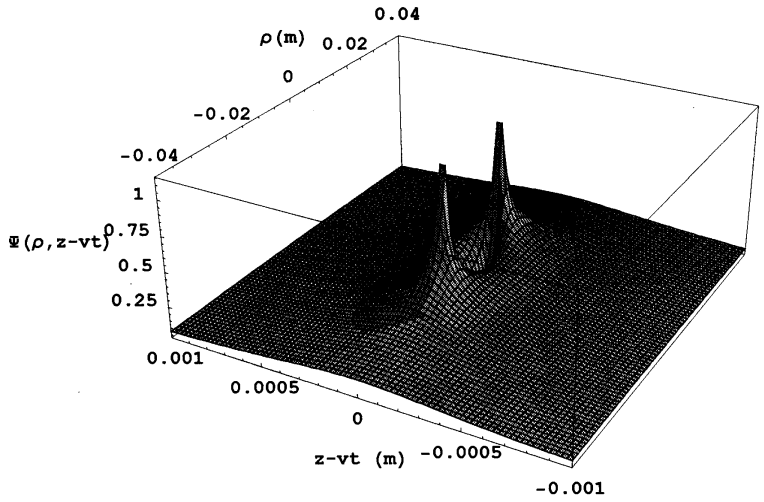

(b) $a_1 = 10^{-5}$ m, $a_2 = 10^{-2}$ m, $\nu/c = 0.9$.

Figure 4(a-b). Surface plot of the real part of the subluminal LW pulse given in Eq. (3.11).

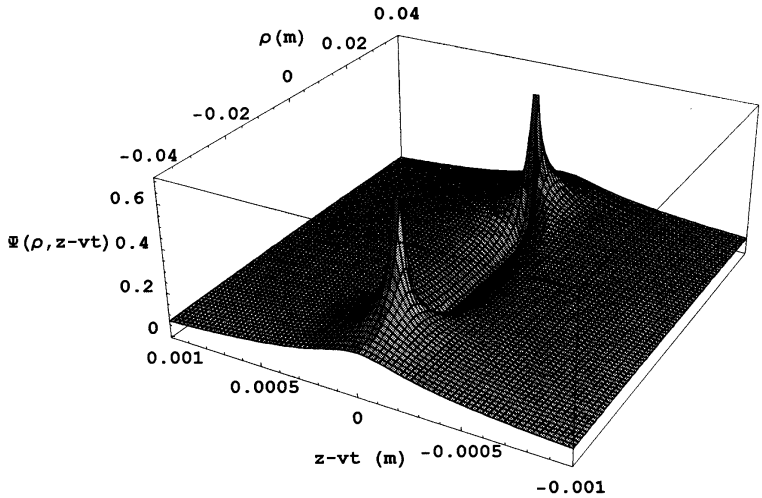

(c) $a_1 = 10^{-5}$ m, $a_2 = 2.5 \times 10^{-2}$ m, $\nu/c = 0.9999$.

Figure 4(c). Surface plot of the real part of the subluminal LW pulse given in Eq. (3.11).

equation. Consider, for example, the following asymmetric solution to the Laplace equation derived by Ziolkowski and Donnelly [43]:

$$\Psi(x,y,z) = \frac{1}{(z_0+z+iy)^{1/2}} e^{-\beta_0 x^2/(z_0+z+iy)} e^{-\beta_0(z-iy)}, \quad \text{for} \quad \beta_0, z_0 > 0. \tag{3.12}$$

Applying a subluminal boost in the z-direction, viz., $z \to \bar{\gamma}(z-\nu t)$, yields the following solution to the 3-D wave equation:

$$\Psi(\vec{r},t) = \frac{1}{(z_0+\bar{\gamma}(z-\nu t)+iy)^{1/2}} e^{-\beta_0 x^2/(z_0+\bar{\gamma}(z-\nu t)+iy)} e^{-\beta_0(\bar{\gamma}(z-\nu t)-iy)}, \quad \text{for} \quad \beta_0, z_0 > 0. \tag{3.13}$$

3.4 Localized Waves Arising from Boosts of the 3-D Helmholtz Equation

In this subsection, we shall obtain LW solutions to the 3-D scalar wave equation by boosting, either subluminally or superluminally,

known stationary solutions of the 3-D Helmholtz equation. Analogous work along these lines has been undertaken previously [cf. e.g., Ref. 49].

We consider the cases of monochromatic solutions to the 3-D wave equation; specifically,

$$\Psi(\rho, z, t) = \phi(\rho, z) e^{i\lambda ct}. \tag{3.14}$$

The function $\phi(\rho, z)$ obeys the Helmholtz equation

$$\left(\nabla_T^2 + \frac{\partial^2}{\partial z^2} + \lambda^2\right) \phi(\rho, z) = 0. \tag{3.15}$$

A specific solution to this equation is given by

$$\phi(\rho, z) = \frac{\sin\left(\lambda\sqrt{\rho^2 + z^2}\right)}{\sqrt{\rho^2 + z^2}}. \tag{3.16}$$

As a consequence, substituting the function (3.16) in Eq. (3.14) and boosting the resulting stationary solution subluminally, we obtain MacKinnon's nondispersive wave packet [89]

$$\Psi(\rho, z, t) = \frac{\sin\left(\lambda\sqrt{\rho^2 + \bar{\gamma}^2(z - \nu t)^2}\right)}{\sqrt{\rho^2 + \bar{\gamma}^2(z - \nu t)^2}} e^{i\lambda\bar{\gamma}(ct - (\nu/c)z)}. \tag{3.17}$$

This solution consists of a localized envelope moving at a subluminal speed multiplied by a plane wave modulation traveling with a superluminal velocity. The envelope of this solution can be written as $j_0\left(\lambda\sqrt{\rho^2 + \bar{\sigma}^2}\right)$, the zeroth order spherical Bessel function of the first kind. This solution can be generalized to a superposition of all spherical modes $j_l(R)Y_{lm}(\theta, \varphi)$, where $Y_{lm}(\theta, \varphi)$ are the spherical harmonics.

4. FINITE ENERGY LOCALIZED WAVES

Traditionally, finite energy LW solutions have been derived using two distinct methods. The first is based on a superposition over particular classes of infinite energy LW solutions. Such a superposition is constructed by integrating over one of the free parameters appearing in

the LW solutions. An example of this procedure is the derivation of the MPS pulse [cf. Eq. (2.8)] by means of a weighted superposition of the basis functions $\Psi_{FWM}(\vec{r}, t; \beta)$ that depend on the free parameter β. The second approach exploits the fact that exact infinite energy LW solutions are nonsingular. Their infinite energy content is a consequence of their boundless extension; i.e., their energy density is finite but space-time is infinite. Consequently, such LW solutions are well behaved on any 2-D surface. For example, infinite energy LW fields on the source plane $z = 0$ are nonsingular and well behaved but their power content does not diminish in time. To obtain planar sources capable of radiating finite energy LW pulses, one can simply time limit the excitation wavefields on the 2-D source plane. This can be done by choosing a suitable time window. This method has been used to derive integral representations of finite time LW solutions [61–64, 69–73, 85–87]. It allows one to work directly with the Fourier spectral content of the initial excitation of a finite energy LW pulsed field. Earlier studies of the generation and propagation of finite time LW and X-wave solutions have demonstrated that they all have unique spatial and temporal spectral structures. Furthermore, it has been shown that the nature of the spectral depletion of LW pulses, as they travel away from their source plane, is different from that of other broadband pulses and quasi-monochromatic signals.

The two approaches discussed in the preceding paragraph are tantamount to introducing some distribution around the conjugate variable frozen by the delta functions appearing in the singular spectra of infinite energy LW pulsed solutions. Consider, for example, the singular spectra given in Eqs. (2.4) and (2.20). In the former case, the Dirac delta function restricts the characteristic variable η to appear only as a phase factor; as a consequence, the localized envelope of the FWM solution depends solely on the other characteristic variable ζ and propagates along this characteristic without any dispersion. The same applies to the singular distribution $\delta(\kappa)$ appearing in the spectrum given in Eq. (2.20). Since this spectrum restricts κ to be equal to zero, the associated boost variable σ does not appear in the resulting X-wave solution. It is clear from this discussion that allowing "frozen" spectral parameters to spread over continuous ranges results in LW solutions having envelopes dependent on both characteristic variables η and ζ, or, alternatively, envelopes that are functions of the two boost variables σ and τ. As they propagate in free-space, such solutions

eventually decay beyond a certain range.

To clarify this issue, we start with the superluminal boost representation given in Eq. (2.19). The introduction of the new variable $\chi' = \sqrt{1 + (\chi/\kappa)^2}$ yields the expression

$$\Psi(\rho, \sigma, \tau) = \int_{-\infty}^{+\infty} d\kappa \int_{1}^{\infty} d\chi' \chi' J_0 \left(\beta \rho \sqrt{\chi'^2 - 1} \right) e^{+i\kappa\sigma} e^{+i\kappa\chi'\tau} \kappa^2 \tilde{\Phi}(\chi', \kappa). \tag{4.1}$$

Next, we choose the specific spectrum

$$\tilde{\Phi}(\chi', \kappa) = \phi(\kappa) e^{-a_1 \kappa \chi'} / \kappa^2 \chi', \quad a_1 > 0, \tag{4.2}$$

where $\phi(\kappa)$ is a well behaved function that allows for a spread in the values of κ. The substitution of the spectrum (4.2) and the use of identify (6.646) in Gradshteyn and Ryzhik [90] reduces the integral in (4.1) to the following form:

$$\Psi(\rho, \sigma, \tau) = \int_{-\infty}^{+\infty} d\kappa \phi(\kappa) \frac{1}{\kappa \sqrt{\rho^2 + (a_1 - i\tau)^2}} e^{-\kappa \sqrt{\rho^2 + (a_1 - i\tau)^2}} e^{+i\kappa\sigma}. \tag{4.3}$$

It is interesting to note that for the singular spectrum $\phi(\kappa) = \kappa_0 \delta(\kappa - \kappa_0)$ we obtain a new infinite energy LW solution; specifically,

$$\begin{aligned} \Psi_{FXW}(\rho, z, t) = & \frac{1}{\sqrt{\rho^2 + (a_1 + i\gamma(z - \nu t))^2}} \\ & \cdot e^{-\kappa_0 \sqrt{\rho^2 + (a_1 + i\gamma(z - \nu t))^2}} e^{+i\kappa_0 \gamma((\nu/c)z - ct)}, \end{aligned} \tag{4.4}$$

where $\gamma = 1/\sqrt{(\nu/c)^2 - 1} > 0$ and $(\nu/c) > 1$. This pulse combines features appearing in both the X-wave and the FWM pulsed fields. We choose to call it the Focused X-wave (FXW) pulse. It resembles the X-wave, except that its highly focused central portion has a tight exponential transverse localization in contrast to the loose algebraic transverse dependence of the X-wave. This behavior results in X-wave-type solutions with lower sidelobes, a property that can significantly improve their resolution when applied to pulse echo techniques used in medical imagine [47]. When compared with the FWM solution given in Eq. (2.5), the FXW appears to have the same form. It consists of

a dispersion-free envelope depending on the boost variable $\gamma(z-\nu t)$ multiplied by an oscillatory term, which is a function of the other boost variable $\gamma((\nu/c)z-ct)$. The FWM given in Eq. (2.5) has a similar structure except that the envelope and the modulation factor depend on the forward and backward traveling characteristic variables $(z-ct)$ and $(z+ct)$, respectively. Another common feature between the FXW and FWM is that both regenerate periodically along the axial z-direction. This can be seen from the surface plots of the FXW shown in Figs. (5.a–e) for different distances $\nu t = 2n\pi(\nu/c)/\kappa_0$. From the figures, it is seen that the FXW is localized at the center and has tails similar to those of the FWM. Another feature is that the center of the envelope of the FXW moves at superluminal speeds $\nu > c$ like the X-wave. Figs. (5.a–e) show the periodic regeneration of the FXW pulse at distances corresponding to $n = 0\,,\ 1/8\,,\ 1/4\,,\ 3/8$ and $1/2$. The length of the focused portion of the pulse depends on the ratio ν/c. The pulse becomes larger as ν/c increases. The radius of the FXW pulse is of the order of a_1.

The envelope and modulation of the FXW seem to be moving in the same direction but at different speeds; however, the superposition (4.1) indicates that this solution consists of forward and backward traveling components. This feature is a prevailing property of all FWM-like solutions. In contrast, the X-wave does not contain backward traveling components because the $\delta(\kappa)$ term in the spectrum (2.20) eliminates the modulation factor that depends on one of the boost variables. In most situations, we would be interested in generating FXW pulses that are predominantly moving in the forward direction. This can be achieved by controlling the parameters appearing in the solution in order to ensure that most of the spectral components contributing to the pulse are moving in one direction. Along this vein, consider the superposition (4.1) consisting of plane waves moving in the z-direction with the χ'–dependent speeds $V(\chi') = c(1-(\nu/c)\chi')/((\nu/c)-\chi')$. Spectral components in the regime $(\nu/c) > \chi' > 1$ travel in the backward direction. On the other hand, spectral components for which $\chi' > (\nu/c)$ acquire positive $V(\chi')$ values; i.e., they travel in the forward direction. Since $\chi' = 1$ is the minimum value contributing to the integration (4.1), values of ν larger but very close to c guarantee that most of the spectral components are moving in the positive z-direction. This condition ensures that a causally generated FXW pulse is a close approximation to the exact pulsed solution given in Eq. (4.4).

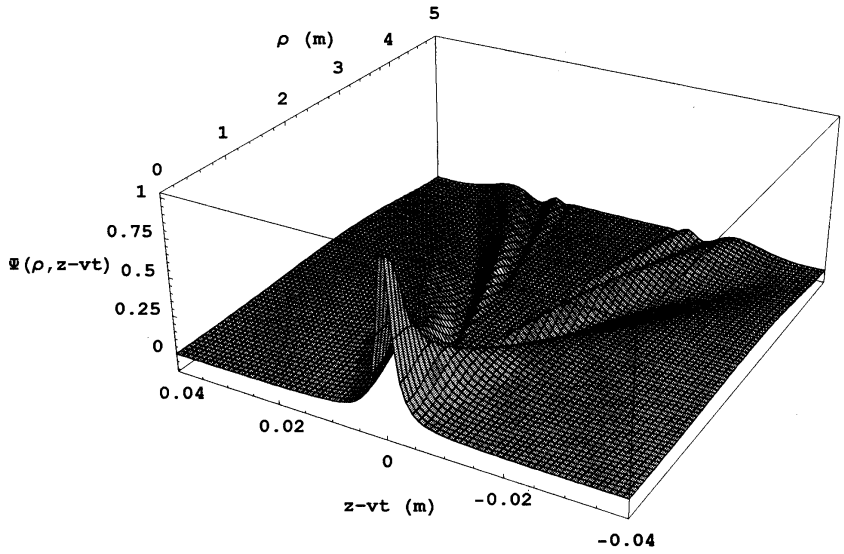

(a) $\nu t = 0$ m.

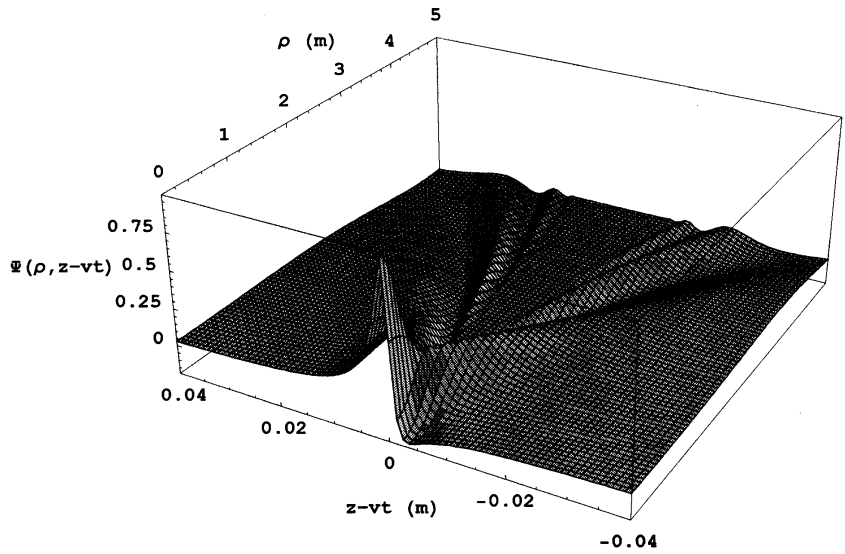

(b) $\nu t = (\pi/4) \times 70.71$ m.

Figure 5(a-b). Surface plot of the real part of the superluminal Focus X-Wave (FXW) pulse with parameters $a_1 = 1$ m, $\kappa_0 = 10$ m^{-1}, $\nu/c = 1.000001$.

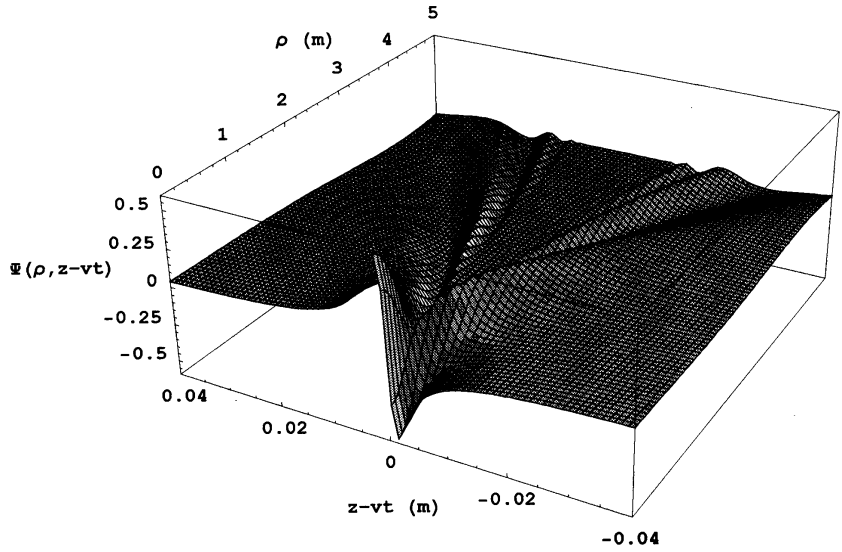

(c) $\nu t = (\pi/2) \times 70.71$ m.

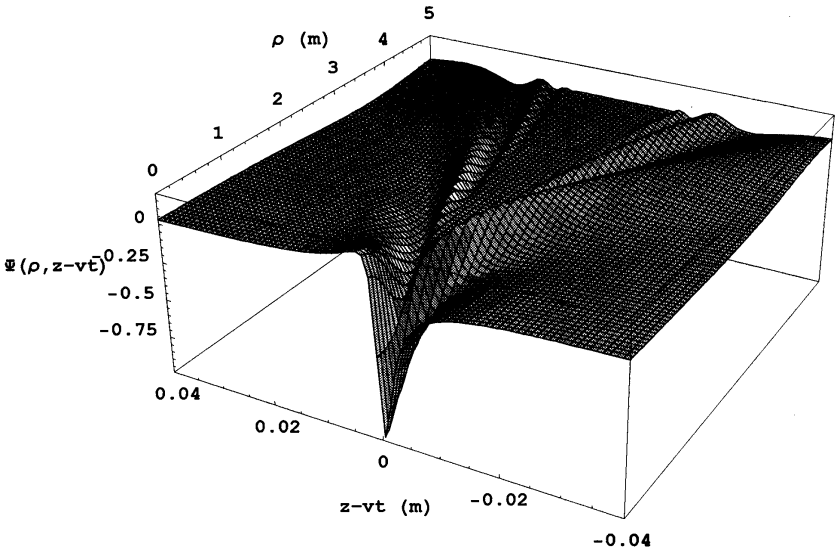

(d) $\nu t = (3\pi/4) \times 70.71$ m.

Figure 5(c-d). Surface plot of the real part of the superluminal Focus X-Wave (FXW) pulse with parameters $a_1 = 1$ m, $\kappa_0 = 10$ m^{-1}, $\nu/c = 1.000001$.

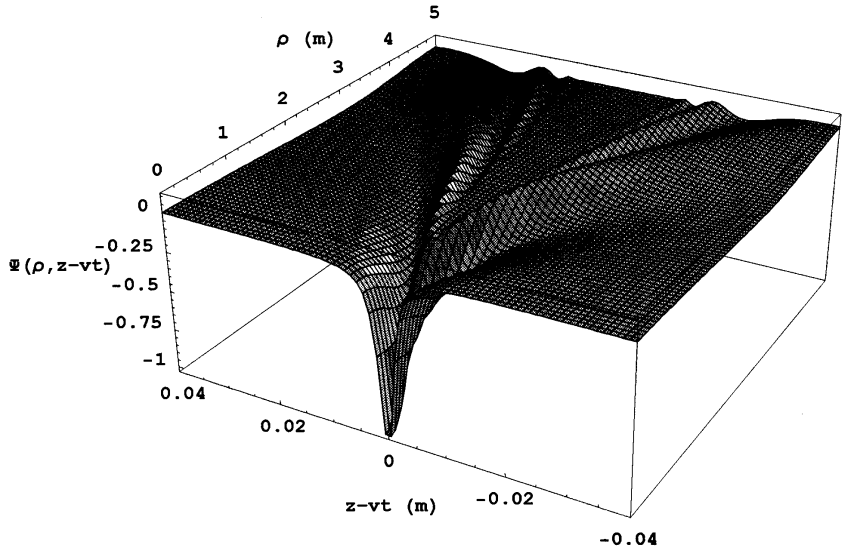

(e) $\nu t = \pi \times 70.71$ m.

Figure 5(e). Surface plot of the real part of the superluminal Focus X-Wave (FXW) pulse with parameters $a_1 = 1$ m, $\kappa_0 = 10$ m^{-1}, $\nu/c = 1.000001$.

One should observe that Eq. (4.3) is a Laplace-type integral. As a consequence, the use of a table of Laplace transforms to evaluate (4.3) can generate a large number of finite energy LW solutions. As an example of a finite energy LW solution derived as a superposition over FXW solutions, we use a spectrum analogous to that of the MPS pulse; specifically,

$$\phi(\kappa) = \begin{cases} \frac{1}{\Gamma(q)}(\kappa - b)^{q-1} e^{-a_2(\kappa - b)} & \text{for } \kappa \geq b, \\ 0 & \text{for } b > \kappa > 0, \end{cases} \tag{4.5}$$

where $q, a_2 > 0$. Substituting this spectrum in Eq. (4.3) and consulting a Laplace transform table, we obtain the Modified Focused X-wave (MFXW) finite energy solution

$$\Psi_{MFXW}(\rho,z,t) = \frac{1}{\left[\sqrt{\rho^2+(a_1-i\tau)^2}+(a_2-i\sigma)\right]^q} \cdot \frac{1}{\sqrt{\rho^2+(a_1-i\tau)^2}} e^{-b\sqrt{\rho^2+(a_1-i\tau)^2}} e^{+ib\sigma}. \quad (4.6)$$

Fig. (6) shows the real part of the MFXW pulse at $\nu t = \gamma 2n\pi/b$, with the parameter values $a_1 = 10^{-2}$ m, $a_2 = 10^{-3}$ m, $(\nu/c) = 1.0001$, $q = 1$ and $b = 1$. One should note that this pulse has the same X-shaped branches that characterize the X-wave. It is clear that this pulse holds out to large distances before it starts decaying. Furthermore, the focused envelope of the pulse does not undergo any major deformation as it decays with distance.

To derive finite energy subluminal X-wave type solutions, one may start with the subluminal boost superposition given in Eq. (2.15) and proceed as in the superluminal case considered in the earlier part of this section. Alternatively, one can start with any of the solutions derived in Sec. 3 and use the invariance properties of the wave equation. An interesting possibility is to consider finite energy solutions that are weighted superpositions of MacKinnon's nondispersive wave packets given in Eq. (3.17), viz.,

$$\Psi(\rho,z,t) = \int_{-\infty}^{+\infty} d\lambda \phi(\lambda) \frac{\sin\left(\lambda\sqrt{\rho^2+\bar{\gamma}^2(z-\nu t)^2}\right)}{\sqrt{\rho+\bar{\gamma}^2(z-\nu t)^2}} e^{i\lambda\bar{\gamma}(ct-(\nu/c)z)}. \quad (4.7)$$

For the specific spectrum

$$\phi(\lambda) = \frac{e^{-a_2\lambda}}{\lambda}\mathbf{H_s}(\lambda), \quad (4.8)$$

where $\mathbf{H_s}(\lambda)$ is the Heaviside unit step function, the integration over λ can be carried out using entry (16) on p. 152 in Erdelyi [91]. The final result is given as follows:

$$\Psi(\rho,z,t) = \frac{1}{\sqrt{\rho^2+\bar{\gamma}^2(z-\nu t)^2}} \arctan\left[\frac{\sqrt{\rho^2+\bar{\gamma}^2(z-\nu t)^2}}{\left(a_2 - i\bar{\gamma}(ct-(\nu/c)z)\right)}\right]. \quad (4.9)$$

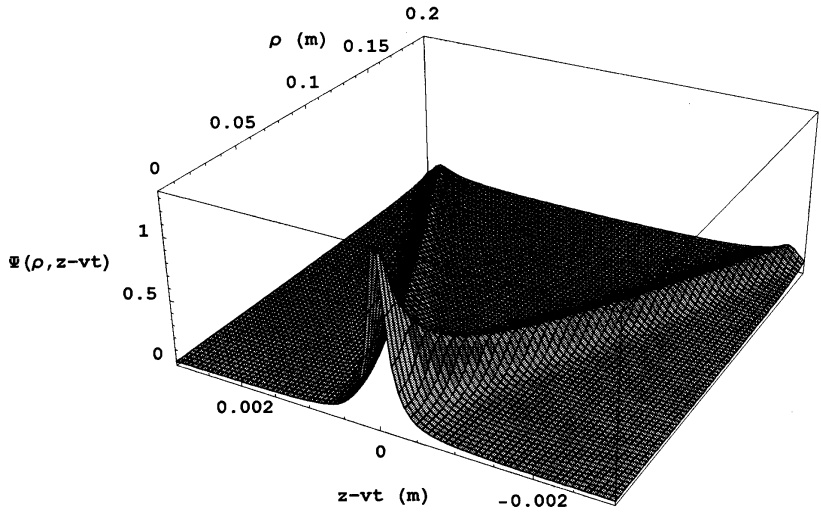

(a) $\nu t = 0$ m.

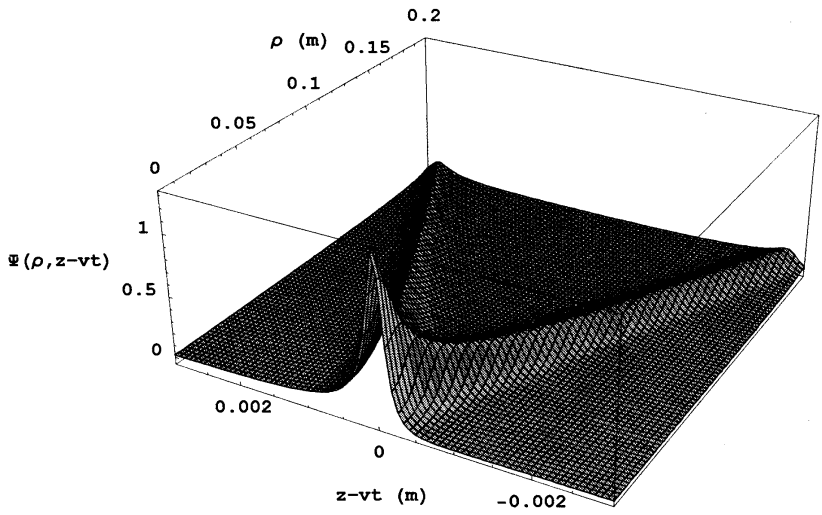

(b) $\nu t = 100\pi \times 70.71$ m.

Figure 6(a-b). Surface plot of the real part of the superluminal Modified Focus X-Wave (MFXW) pulse with parameters $b = 1$ m^{-1}, $a_1 = 10^{-2}$ m, $a_2 = 10^3$ m, and $\nu/c = 1.0001$.

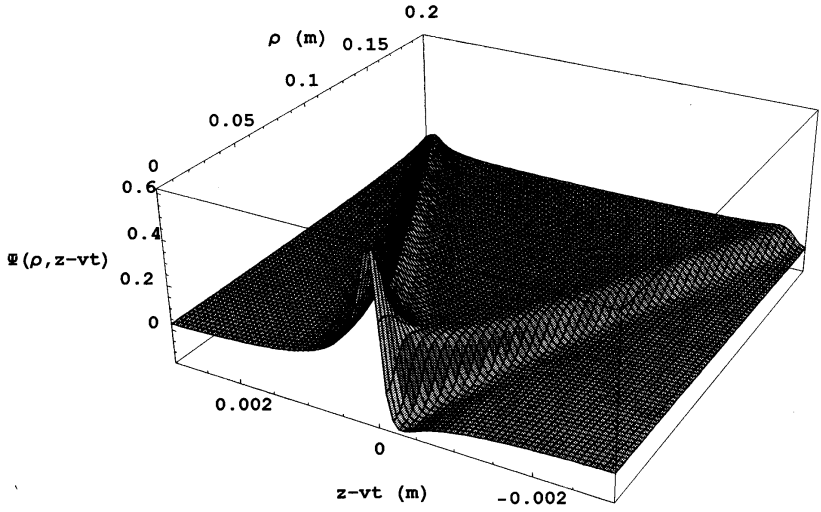

(c) $\nu t = 500\pi \times 70.71$ m.

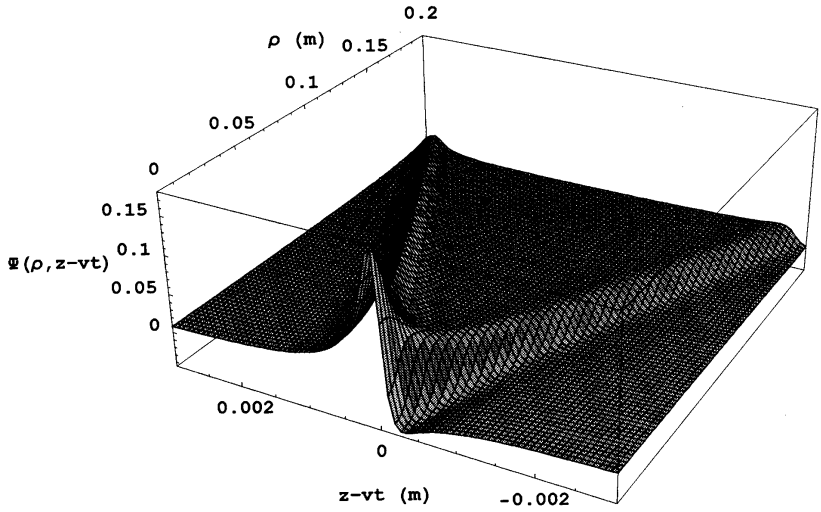

(d) $\nu t = 2000\pi \times 70.71$ m.

Figure 6(c-d). Surface plot of the real part of the superluminal Modified Focus X-Wave (MFXW) pulse with parameters $b = 1$ m^{-1}, $a_1 = 10^{-2}$ m, $a_2 = 10^3$ m, and $\nu/c = 1.0001$.

This is a well behaved nonsingular solution representing a wavepacket moving at a subluminal speed $\nu < c$, but modified by the presence of the second boost variable $\bar{\gamma}(ct - (\nu/c)z)$. This solution can be made "almost undistorted" by choosing ν slightly smaller than c. Plots of this new solution are shown in Fig. (7) for $a_2 = 0.1$ m and $(\nu/c) = 0.99999$ at distances $\nu t = 0\,, 100, 500$ and 2000 m. One should note the resemblance of the decay of this pulse to that of the MS pulse illustrated in Fig. (2). This pulse initially has a good localization. It does not branch out in the manner that the X-wave or the FWM pulses do. In addition, the pulse given in (4.9) is more focused at $\nu t = 100$ m than at the origin. This means that the pulse focuses a little before it starts spreading out.

5. BEHAVIOR OF LW FIELDS ON THE SOURCE PLANE $z = 0$

In this section, we would like to discuss some of the aspects related to the behavior of the LW fields on a specific source plane. Toward this goal, it is useful to introduce the following Fourier representation of solutions to the scalar wave equation:

$$\Psi(\rho, z, t) = \int_{-\infty}^{+\infty} dk_z \int_{-\infty}^{+\infty} d\omega \int_{0}^{\infty} d\chi \chi J_0(\chi\rho) e^{+i\omega t} e^{-ik_z z} \cdot \Phi_F(\chi, k_z, \omega) \delta\left((\omega/c)^2 - k_z^2 - \chi^2\right). \tag{5.1}$$

It has already been mentioned that one can transform the bidirectional superposition given in Eq. (2.2) to the Fourier superposition given in Eq. (5.1) using the change of variables $\alpha = ((\omega/c) + k_z)/2$ and $\beta = ((\omega/c) - k_z)/2$. Analogously, the subluminal and superluminal superpositions given in Eqs. (2.15) and (2.19), respectively, can be transformed to the Fourier picture using the relations $\kappa = \bar{\gamma}\left((\omega/c) - k_z(\nu/c)\right)$ and $\lambda = \bar{\gamma}\left((\omega/c)(\nu/c) - k_z\right)$ for the subluminal representation, and $\kappa = \gamma\left((\omega/c) - k_z(\nu/c)\right)$ and $\lambda = \gamma((\omega/c)(\nu/c) - k_z)$ for the superluminal one. The Weyl representation, viz.,

$$\Psi(\rho, z, t) = \int_{-\infty}^{+\infty} d\omega \int_{0}^{\infty} d\chi \chi J_0(\chi\rho) e^{-i\sqrt{(\omega/c)^2 - \chi^2}\, z} e^{+i\omega t} \tilde{\Phi}_F(\chi, \omega) \tag{5.2}$$

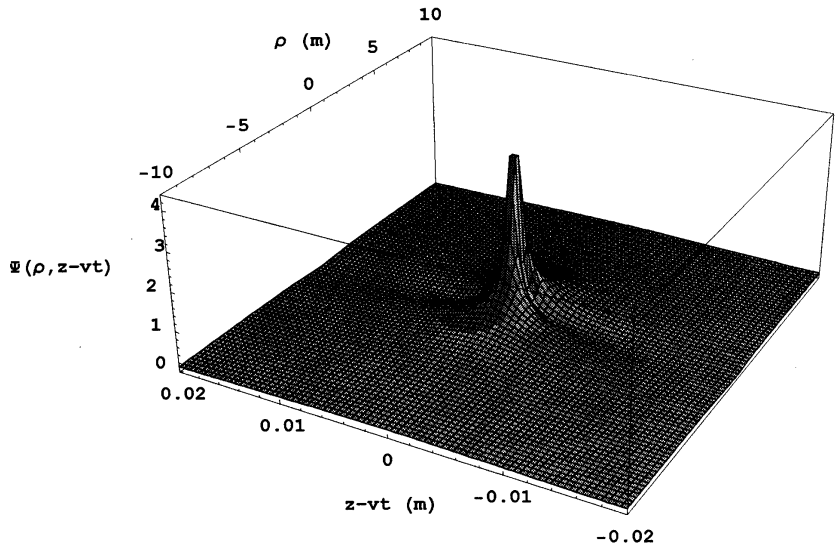

(a) $\nu t = 0$ m.

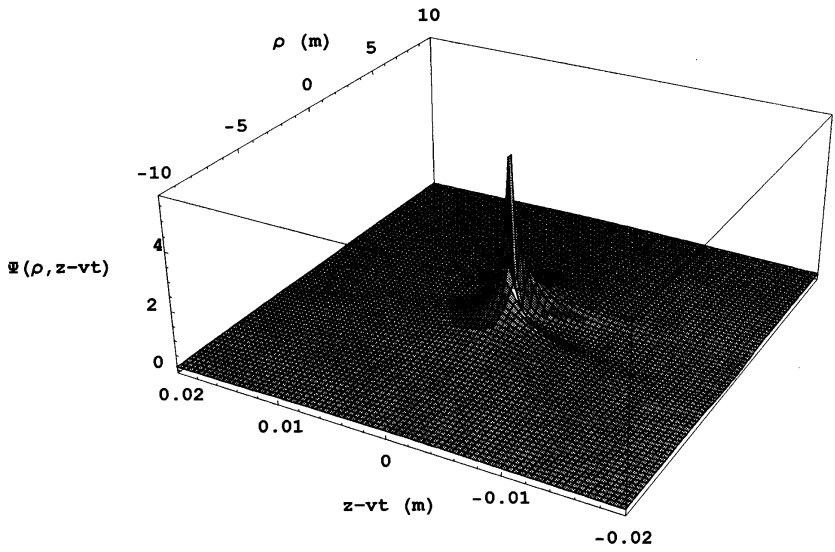

(b) $\nu t = 100$ m.

Figure 7(a-b). Surface plot of the real part of the subluminal pulse given in Eq. (4.9) with parameters $a_2 = 0.1$ m, and $\nu/c = 0.99999$.

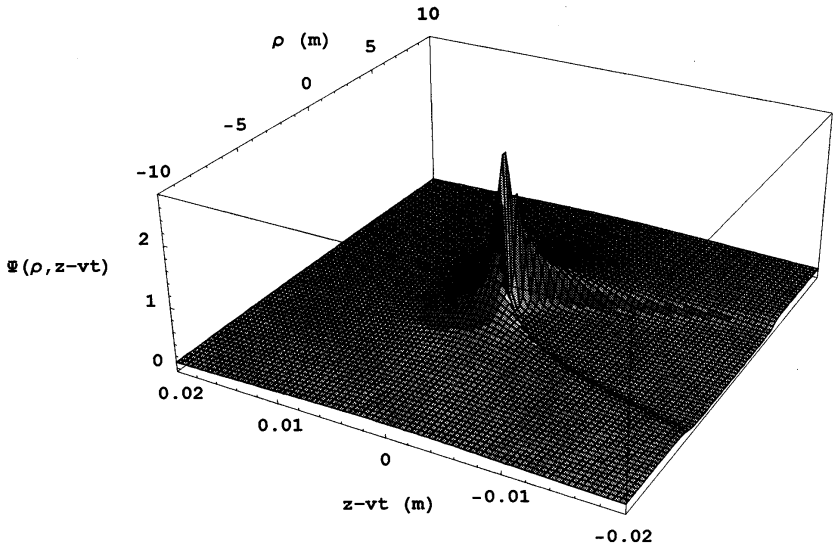

(c) $\nu t = 500$ m.

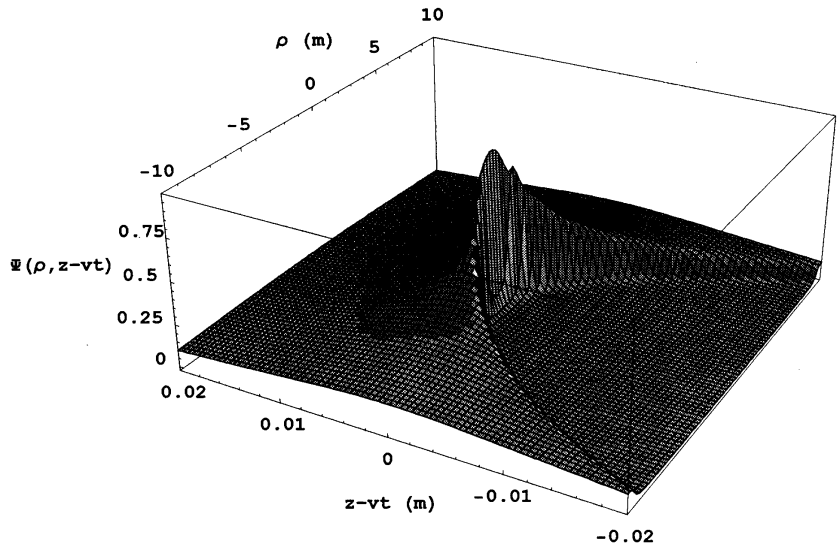

(d) $\nu t = 2000$ m.

Figure 7(c-d). Surface plot of the real part of the subluminal pulse given in Eq. (4.9) with parameters $a_2 = 0.1$ m, and $\nu/c = 0.99999$.

follows from carrying out the integration over k_z in Eq. (5.1). Using the aforementioned connection between the Fourier and the boost spectral variables, we can show that the Fourier spectrum of the infinite energy X-wave pulse (2.23) has the following form:

$$\tilde{\Phi}_F(\omega, \chi) = \delta(\omega - \gamma\nu\chi)e^{-\chi a_1}/\chi. \tag{5.3}$$

To obtain finite energy X-waves, we can replace the Dirac delta function in (5.3) by a continuous Gaussian distribution. Specifically, we choose

$$\tilde{\Phi}_F(\omega, \chi) = \hat{\delta}(\omega - \gamma\nu\chi)e^{-\chi a_1}/\chi, \tag{5.4a}$$

where

$$\hat{\delta}(\omega - \gamma\nu\chi) = \frac{T}{\sqrt{\pi}}e^{-T^2(\omega-\gamma\nu\chi)^2}. \tag{5.4b}$$

Introducing this spectrum into expression (5.2), we have

$$\Psi(\rho, z, t) = \frac{T}{\sqrt{\pi}} \int_{-\infty}^{+\infty} d\omega \int_0^{\infty} d\chi\chi J_0(\chi\rho)e^{-i\sqrt{(\omega/c)^2-\chi^2}z}e^{+i\omega t} \times e^{-T^2(\omega-\gamma\nu\chi)^2}\frac{e^{-\chi a_1}}{\chi}. \tag{5.5}$$

Suppose we consider this expression on the aperture plane $z = 0$, viz.,

$$\Psi(\rho, 0, t) = \frac{T}{\sqrt{\pi}} \int_{-\infty}^{+\infty} d\omega \int_0^{\infty} d\chi\chi J_0(\chi\rho)e^{+i\omega t}e^{-T^2(\omega-\gamma\nu\chi)^2}\frac{e^{-\chi a_1}}{\chi}. \tag{5.6}$$

Carrying out the integrations over ω and χ, we obtain

$$\Psi^{(0)}_{XW}(\rho, 0, t) = \frac{1}{(\rho^2 + (a_1 - i\gamma\nu t)^2)^{1/2}}e^{-t^2/4T^2}. \tag{5.7}$$

This is just the infinite energy X-wave field at $z = 0$, time-limited by a Gaussian window.

One should note that any infinite energy X-wave type solution has the form

$$\Phi_2(\rho, t) \equiv \Psi(\rho, 0, t) = \int_0^{\infty} d\chi\chi J_0(\chi, \rho)e^{+i\gamma\nu\chi t}\tilde{\Phi}(\chi) \tag{5.8}$$

at the source plane $z = 0$. This is a solution of the 2-D pseudo-differential equation

$$-i\frac{1}{\gamma\nu}\frac{\partial}{\partial t}\Psi_2(\rho,t) = \sqrt{-\nabla_T^2}\,\Psi_2(\rho,t), \tag{5.9}$$

which governs the complex analytical signal corresponding to the 2-D scalar wave equation

$$\left(\nabla_T^2 - \frac{1}{(\gamma\nu)^2}\frac{\partial^2}{\partial t^2}\right)\Psi_2(\rho,t) = 0. \tag{5.10}$$

An important observation, then, is that the infinite energy X-wave field restricted to the source plane $z = 0$ is a solution to the 2-D scalar wave equation (5.10). This indicates that a spreading 2-D wave solution propagates on the source plane with a velocity $(\gamma\nu)$. This reflects the dynamic character of the illumination of the plane of an X-wave source. It must be emphasized that this behavior is a property only of infinite energy pulses. A finite energy X-wave restricted to the source plane [cf. Eq. (5.7)] is not necessarily a solution of the 2-D wave equation. In most cases, the finite energy solution consists of an infinite energy 2-D wave function multiplied by a time window. This window limits the expansion of the 2-D illumination of the source plane and prevents it from acquiring infinite extension. In Eq. (5.7) the time window is the Gaussian $\exp(-t^2/4T^2)$. Another example is the finite energy solution given in Eq. (4.6). It consists of a product of the infinite energy FXW solution and the time window $\left[\sqrt{\rho^2 + (a_1 - i\gamma\nu t)^2} + (a_2 + i\gamma c t)\right]^{-q}$. The window in this case depends on the transverse radius ρ. This means that distinct annular rings of the source plane are windowed using different time functions.

In a similar fashion, we consider the behavior of FWM-like fields on the source plane $z = 0$. The infinite energy FWM pulse has the Weyl representation

$$\Psi(\rho,z,t) = \int_{-\infty}^{+\infty} d\omega \int_0^{\infty} d\chi\chi J_0(\chi\rho) e^{-i\sqrt{(\omega/c)^2-\chi^2}z} e^{+i\omega t}\tilde{\Phi}_F(\chi,\omega), \tag{5.11a}$$

with the Fourier spectrum

$$\tilde{\Phi}_F(\chi,\omega) = \frac{1}{2\beta} e^{-(\chi^2/4\beta)a_1}\delta\left(\omega - c\left(\left(\chi^2/4\beta\right) + \beta\right)\right). \tag{5.11b}$$

The replacement of the Dirac δ function by a Gaussian function $\hat{\delta}$ [cf. Eq. (5.4b)] produces a finite energy solution. On the source plane ($z = 0$), the finite energy field consists of the infinite energy FWM multiplied by the time window $\exp(-t^2/4T^2)$. In contrast to the X-wave infinite-energy solution, the FWM-like pulse restricted to the source plane does not satisfy the 2-D scalar wave equation. Consider the representation given in (5.11) on the plane $z = 0$. After carrying out the integration over ω , we obtain

$$\Psi_2(\rho, t) \equiv \Psi(\rho, 0, t) = \frac{1}{2\beta} \int_0^\infty d\chi \chi J_0(\chi\rho) e^{+i((\chi^2/3\beta)+\beta)ct} e^{-\chi^2(a_1/4\beta)}. \tag{5.12}$$

This expression is a solution to the Schrödinger equation

$$-i\frac{1}{c}\frac{\partial}{\partial t}\Psi_2(\rho, t) = -\frac{1}{2\beta}\nabla_T^2\Psi_2(\rho, t) + \beta\Psi_2(\rho, t). \tag{5.13}$$

As a consequence, the infinite energy FWM field on the source plane is governed by a 2-D parabolic equation. This means that the dynamic character of the illumination of the FWM aperture is that of a diffusion field. This should be contrasted to the propagating 2-D fields associated with the planar illumination of the X-wave. These differences are reflected also in the corresponding spatio-temporal spectral couplings. The FWM pulse has a spatio-temporal coupling of the form $\omega \propto \chi^2$, while for the X-wave we have $\omega \propto \chi$. The former is basically the dispersion relationship of a parabolic equation, while the latter is the dispersion relation of a first-order hyperbolic equation. A possible extension of our analysis to new LW solutions is to work with a spectral coupling of the form $\omega \propto \chi^n$ for $n > 2$. This will lead to new classes of infinite energy LW solutions for which the illumination of the source planes obeys higher order 2-D partial differential equations.

6. CONCLUDING REMARKS

In this work we have studied two superpostions that are suitable for the derivation of LW solutions to the scalar wave equation. The first uses superpositions over products of plane waves moving in opposite directions along the characteristic variables $(z - ct)$ and $(z + ct)$. This bidirectional representation was introduced in an earlier publication and has proved instrumental in advancing our understanding of the

properties of FWM-like pulses. In this sequel, we have been guided by our previous experience with the bidirectional representation towards a new superposition. The latter uses products of plane waves propagating along the subluminal and superluminal boost variables. This new superposition was motivated by the need to derive new closed-form X-wave type solutions. We were able to extend our previous knowledge of constructing FWM-like solutions to X-wave types because these two classes of wavefields have more common features than differences. They are both highly focused pulses embedded in extended background fields having much lower intensities. The closed-form infinite energy X-wave and FWM pulses have similar spectral structures. Both are characterized by a Dirac delta function that couples their spatial and temporal spectral variables. To obtain finite energy X-wave and FWM pulses, the sharp delta function is smeared. The resulting decay in the amplitudes of the propagating wavefields is caused by a distinctive spectral depletion mechanism shared by the two types of pulses.

The boost representations presented in this paper are based on the Lorentz invariance of the wave equation. This implies that our technique can be easily extended to other Lorentz invariant equations; e.g., the Klein-Gordon or Maxwell's equations. We have elaborated on the use of superluminal and subluminal Lorentz transformations to derive LW solutions to the scalar wave equation by boosting known solutions of other equations. Elementary solutions derived by such a procedure can be superimposed over different spectral distributions to yield a variety of closed- form infinite and finite energy solutions. Several of these have been deduced and their properties have been discussed. It has been shown that the envelope of an infinite energy LW pulse, derived in this manner, depends only on one of the two boost variables. On the other hand, a finite energy pulse is a nonseparable function of the two boost variables. This is analogous to the properties of LW pulses derived using the bidirectional representation. In this case, the envelope of an infinite energy pulse depends on one of the two characteristic variables $(z - ct)$ or $(z + ct)$, while a finite energy solution is a nonseparable function of these two quantities.

The two superpositions studied in this work provide a natural framework for deriving novel LW solutions and subsequently deduce their Fourier spectra. The latter is an important step because ultimately one needs to link the Fourier spectral properties of the LW pulses to the physical characteristics of the sources generating them. In ad-

dition, a study of the depletion of the spectral components provides insight into the propagation characteristics of the LW pulses.

The main thrust of our work has not been to investigate the details of the applicability of the deduced solutions in specific fields. Instead, we have attempted to present a simple and coherent procedure that can be efficiently used to deduce new LW pulses and to comment briefly on their general properties. The strength of our approach is not based only on *retrodiction*, that is the deduction and categorization of already-known solutions. Our approach has an extraordinary power of *prediction*. This power is made evident in this paper by the systematic derivation of a number of new LW solutions. Two of these are finite energy X-wave type of solutions [e.g., Eqs. (4.6) and (4.9)]. To the best of our knowledge these are the first closed-form expressions deduced for finite energy LW pulses of this kind. We anticipate that such new solutions can be studied individually and that detailed future comparisons can lead to more insights concerning possible fields of application. Specifically, we hope that certain features exhibited by these pulses can be beneficial to the advancement of the applicability of LW pulses.

The generation of LW pulses may be understood as a result of an initial illumination of an aperture plane. On such a source surface, the power of the initial excitation of an infinite energy LW pulse is always finite. The energy becomes infinite because the aperture is illuminated for an infinite period of time. To obtain finite energy LW pulses one may turn off the illumination field at a certain time. This procedure has been studied in previous publications [61–64, 69–73, 85–87]. However, in this paper we have investigated the behavior of the illumination fields on the generating aperture. We have shown, specifically, that whereas the infinite energy FWM on the source plane obeys a 2-D parabolic Shrodinger-like equation, the X-wave obeys a 2-D scalar wave equation. This is a consequence of their specific spatio-temporal spectral couplings. Finite energy solutions obtained by smearing the spectral delta functions consist of two terms. One is still a solution of the 2-D parabolic or the 2-D scalar wave equation, while the other represents a time window that ultimately turns off the power of the illumination wavefield.

REFERENCES

1. Brittingham, J. N., "Focus wave modes in homogeneous Maxwell equations: Transverse electric mode," *J. Appl. Phys.*, Vol. 54, 1179–1189, 1983.
2. Wu, T. T., and R. W. P. King, "Comments on focus wave modes in homogeneous Maxwell equations: Transverse electric mode," *J. Appl. Phys.*, Vol. 56, 2587, 1984.
3. Belanger, P. A., "Packetlike solutions of the homogeneous wave equation," *J. Opt. Soc. Am.*, Vol. A1, 723, 1984.
4. Wu, T. T., "Electromagnetic missiles," *J. Appl. Phys.*, Vol. 57, 2370, 1985.
5. Ziolkowski, R. W., "Exact solutions of the wave equation with complex source locations," *J. Math. Phys.*, Vol. 26, 861–863, 1985.
6. Sezginer, A., "A general formulation of focus wave modes," *J. Appl. Phys.*, Vol. 57, 678, 1985.
7. Wu, T. T., and H. Lehmann, "Spreading of electromagnetic pulses," *J. Appl. Phys.*, Vol. 58, 2064, 1985.
8. Moses, H. E., and R. T. Prosser, "Initial conditions, sources, and currents for prescribed time-dependent acoustic and electromagnetic fields in three dimensions, Part I: The inverse initial value problem. Acoustic and electromagnetic 'bullets,' expanding waves, and imploding waves," *IEEE Trans. Antennas Propag.*, Vol. AP-34, 188–196, 1986.
9. Belanger, P. A., "Lorentz transformation of the particlelike solutions of the homogeneous wave equation," *J. Opt. Soc. Am.*, Vol. A3, 541, 1986.
10. Hillion, P., "Spinor focus wave modes," *J. Math. Phys.*, Vol. 28, 1743, 1987.
11. Heyman, E., B. Z. Steinberg, and L. B. Felsen, "Spectral analysis of focus wave modes," *J. Opt. Soc. Am.*, Vol. A4, 2081, 1987.
12. Durnin, J., "Exact solutions for nondiffracting beams. I. The scalar theory," *J. Opt. Soc. Am.*, Vol. A4, 651–654, 1987.
13. Durnin, J., J. J. Miceli, Jr., and J. H. Eberly, "Diffraction free beams," *Phys. Rev. Lett.*, Vol. 58, 1499–1501, 1987.
14. Hillion, P., "Splash wave modes in homogeneous Maxwell equations," *J. Electromagnetic Waves Appl.*, Vol. 2, 725–739, 1988.
15. Besieris, I. M., A. M. Shaarawi, and R. W. Ziolkowski, "A bidirectional traveling plane wave representation of exact solutions of the scalar wave equation," *J. Math. Phys.*, Vol. 30, 1254–1269, 1989.

16. Shaarawi, A. M., I. M. Besieris, and R. W. Ziolkowski, "Localized energy pulse trains launched from an open, semi-infinite, circular waveguide," *J. Appl. Phys.*, Vol. 65, 805–813, 1989.
17. Ziolkowski, R. W., A. M. Shaarawi, and I. M. Besieris, "A space-time representation of a massive, relativistic, spin-zero particle," *Nuclear Phys.*, Vol. B6, 255–258, 1989.
18. Ziolkowski, R. W., "Localized transmission of electromagnetic energy," *Phys. Rev.*, Vol. A39, 2005–2033, 1989.
19. Ziolkowski, R. W., D. K. Lewis, and B. D. Cook, "Experimental verification of the localized wave transmission effect," *Phys. Rev. Lett.*, Vol. 62, 147–150, 1989.
20. Heyman, E., "Focus wave modes: A dilemma with causality," *IEEE Trans. Antennas and Propagat.*, Vol. 37, 1604, 1989.
21. Shaarawi, A. M., *Nondispersive Wavepackets*, Ph. D. Thesis, Virginia Polytechnic Institute and State University, Blacksburg, Virginia (1989).
22. Ziolkowski, R. W., and D. K. Lewis, "Verification of the localized wave transmission effect," *J. Appl. Phys.*, Vol. 68, 6083–6086, 1990.
23. Shaarawi, A. M., I. M. Besieris, and R. W. Ziolkowski, "A novel approach to the synthesis of nondispersive wave packet solutions to the Klein-Gordon and Dirac equations," *J. Math. Phys.*, Vol. 31, 2511–2519, 1990.
24. Ziolkowski, R. W., "Localized wave physics and engineering," *Phys. Rev.*, Vol. A44, 3960–3984, 1991.
25. Ziolkowski, R. W. I. M. Besieris, and A. M. Shaarawi, "Localized wave representations of acoustic and electromagnetic radiation," *Proc. IEEE*, Vol. 79, 1371–1378, 1991.
26. Tippet, M. K., and R. W. Ziolkowski, "A bidirectional wave transformation of the cold plasma equations," *J. Math. Phys.*, Vol. 32, 488–492, 1991.
27. Ziolkowski, R. W., and M. K. Tippet, "Collective effect in an electron plasma system catalyzed by a localized electromagnetic wave," *Phys. Rev.*, Vol. A43, 3941–3947, 1991.
28. Overfelt, P. L., "Bessel-Gauss pulses," *Phys. Rev.*, Vol. A44, 3941–3947, 1991.
29. Hafizi, B., and P. Sprangle, "Diffraction effects in directed radiation beams," *J. Opt. Soc. Am.*, Vol. Vol. A8, 705–717, 1991.
30. Vengsarkar, A. M., I. M. Besieris, A. M. Shaarawi, and R. W. Ziolkowski, "Closed-form localized wave solutions in optical fiber waveguides," *J. Opt. Soc. Am.*, Vol. A9, 937–949, 1992.
31. Hernandez, J. E., R. W. Ziolkowski, and S. Parker, "Synthesis of the driving functions of an array for propagating localized waves,"

J. Acoust. Soc. Am., Vol. 92, 550, 1992.
32. Ziolkowski, R. W., "Properties of electromagnetic beams generated by ultrawide bandwidth pulse driven arrays," *IEEE Trans. Antennas Propagat.*, Vol. 40, 888, 1992.
33. Donnelly, R., and R. Ziolkowski, "A method for constructing solutions of homogeneous partial differential equations: Localized waves," *Proc. R. Soc. Lond.*, Vol. A437, 677–692, 1992.
34. Lu, J. Y., and J. F. Greenleaf, "Nondiffracting X waves – exact solutions to free space scalar wave equations and their finite aperture realization," *IEEE Trans. Ultrason. Ferroelec. Freq. Contr.*, Vol. 39, 19–31, 1992.
35. Lu, J. Y., and J. F. Greenleaf, "Experimental verification of nondifracting X waves," *IEEE Trans. Ultrason. Ferroelec. Freq. Contr.*, Vol. 39, 441–446, 1992.
36. Lu, J. Y., and J. F. Greenleaf, "Diffraction-limited beams and their applications for ultrasonic imaging and tissue characterization," *Proc. SPIE*, Vol. 1733, 92–119, 1992.
37. Hillion, P., "Nondispersive waves: Interpretation and causality," *IEEE Trans. Antennas Propagat.*, Vol. 40, 1031, 1992.
38. Hillion, P., "Focus wave modes and diffraction of plane waves," *J. Opt.* (Paris), Vol. 23, 233–235, 1992.
39. Hillion, P., "Nondispersive solutions of the Klein-Gordon equation," *J. Math. Phys.*, Vol. 33, 1817-1821, 1992.
40. Hillion, P., "Nondispersive solutions of the Dirac equation," *J. Math. Phys.*, Vol. 33, 1822–1830, 1992.
41. Ziolkowski, R. W., I. M. Besieris, and A. M. Shaarawi, "Aperture realizations of the exact solutions to homogeneous-wave equations," *J. Opt. Soc. Am.*, Vol. A10, 75–87, 1993.
42. Palmer, M. R., and R. Donnelly, "Focused wave modes and the scalar wave equation," *J. Math. Phys.*, Vol. 34, 4007–4013, 1993.
43. Donnelly, R., and R. Ziolkowski, "Designing localized waves," *Proc. R. Soc. Lond.*, Vol. A440, 541–565, 1993.
44. Power, D., R. Donnelly, and R. MacIsaac, "Spherical scattering of superpositions of localized waves," *Phys. Rev.*, Vol. E48, 1410–1417, 1993.
45. Overfelt, P. L., "Continua of localized wave solutions via complex similarity transformations," *Phys. Rev.*, Vol. E47, 4430–4438, 1993.
46. Borisov, V. V., and A. B. Utkin, "Electromagnetic fields produced by the spike pulse of hard radiation," *J. Phys. A: Math. Gen.*, Vol. 26, 4081–4085, 1993.
47. Lu, J. Y., and J. F. Greenleaf, "Sidelobe reduction for limited diffraction pulse-echo system," *IEEE Trans. Ultrason. Ferroelec.*

Freq. Contr., Vol. 30, 735–746, 1993.
48. Hillion, P., "How do focus wave modes propagate across a discontinuity in a medium?" *Optik*, Vol. 93, 67–72, 1993.
49. Barut, A. O., G. D. Maccarone, and E. Recami, "On the shape of tachyons," *Il Nuovo Cimento,* Vol. 71, 509–533, 1982; Recami, E., "Classical tachyons and possible applications," *Rivista del Nuovo Cimento,* Vol. 9, 1–178, 1986; Barut, A. O., and H. C. Chandola, "Localized tachyonic wavelet solutions to the wave equation," *Phys. Lett. A*, Vol. 180, 5–8, 1993.
50. Besieris, I. M., A. M. Shaarawi, and R. W. Ziolkowski, "Nondispersive accelerating wavepackets," *Am. J. Phys.*, Vol. 62, 519–521, 1994.
51. Shaarawi, A. M., I. M. Besieris, and R. W. Ziolkowski, "Diffraction of a nondispersive wavepacket in a two slit interference experiment," *Phys. Lett.*, Vol. A188, 218–224, 1994.
52. Donnelly, R., D. Power, G. Templeman, and A. Whalen, "Graphic simulation of superluminal acoustic localized wave pulses," *IEEE Trans. Ultrason. Ferroelec. Freq. Contr.*, Vol. 41, 7–12, 1994.
53. Overfelt, P. L., "On the possibility of localized wave propagation using a classical two-fluid model of superconductors," *J. Math. Phys.*, Vol. 35, 2233–2258, 1994.
54. Heyman, E., and L. B. Felsen, "Comment on 'Nondispersive waves: Interpretation and causality,' by P. T. M. Hillion," *IEEE Trans. Antennas Propagat.*, Vol. 42, 1668, 1994.
55. Borisov, V. V., and A. B. Utkin, "Some solutions to the wave and Maxwell's equations," *J. Math. Phys.*, Vol. 35, 3624–3630, 1994.
56. Lazarev, Y. N., and P. V. Petrov, "Generation of an intense directed ultra-short electromagnetic pulse," *JETP Lett.*, Vol. 60, 634–638, 1994.
57. Borisov, V. V., and A. B. Utkin, "Focus wave modes in conducting media," *Can. J. Phys.*, Vol. 72, 293, 1994.
58. Borisov, V. V., and A. B. Utkin, "Focus wave modes in noncollisional plasma," *Can. J. Phys.*, Vol. 72, 647, 1994.
59. Borisov, V. V., and A. B. Utkin, "On the formation of focus wave modes," *J. Phys. A: Math. Gen.*, Vol. 27, 2587–2591, 1994.
60. Lu, J. Y., H. Zou, and J. F. Greenleaf, "Biomedical beam forming," *Ultrasound Med. Biol.*, Vol. 20, 403–428, 1994.
61. Chatzipetros, A. A., *Sources of Localized Waves*, Ph.D. Thesis, Virginia Polytechnic Institute and State University, Blacksburg, Virginia, 1994.
62. Shaarawi, A. M., I. M. Besieris, and R. W. Ziolkowski, "The

propagating and evanescent field components of localized wave solutions," *Opt. Comm.*, Vol. 116, 183–192, 1995.
63. Shaarawi, A. M., R. W. Ziolkowski, and I. M. Besieris, "On the evanescent fields and the causality of the focus wave modes," *J. Math. Phys.*, Vol. 36, 5565–5587, 1995.
64. Shaarawi, A. M., I. M. Besieris, R. W. Ziolkowski, and S. M. Sedky, "Generation of approximate focus wave mode pulses from wide-band dynamic Gaussian aperture," *J. Opt. Soc. Am.*, Vol. A12, 1954–1964, 1995.
65. Lu, J. Y., H. Zou, and J. F. Greenleaf, "A new approach to obtain limited diffraction beams," *IEEE Trans. Ultrason. Ferroelec. Freq. Contr.*, Vol. 42, 850–853, 1995.
66. Lu, J. Y., "Bowtie limited diffraction beams for low-sidelobe and large depth of field imagine," *IEEE Trans. Ultrason. Ferroelec. Freq. Contr.*, Vol. 42, 1050–1063, 1995.
67. Lu, J. Y., and J. F. Greenleaf, "Comparison of sidelobes of limited diffraction beams and localized waves," *Acoust. Imag.*, J. P. Jones, Ed., Vol. 22, 145–162, 1995.
68. Sun, J., *Acoustic Bullets: Generation and Propagation*, Ph.D. Thesis, University of Rhode Island, 1995.
69. Sedky, S. M., *Generation of Localized Waves Using Dynamic Apertures*, M. Sc. Thesis, Cairo University, Giza, Egypt, 1995.
70. Shaarawi, A. M., S. M. Sedky, R. W. Ziolkowski, and I. M. Besieris, "The spatial distribution of the illumination of dynamic apertures and its effect on the decay rate of the radiated localized pulses," *J. Phys. A: Math. Gen.*, Vol. 29, 5157–5179, 1996.
71. Shaarawi, A. M., S. M. Sedky, R. W. Ziolkowski, and F. M. Taiel, "Effect of the switching pattern of the illumination of dynamic apertures on the ranges of the generated waves," *J. Opt. Soc. Am.*, Vol. A13, 1712–1718, 1996.
72. Shaarawi, A. M., S. M. Sedky, F. M. Taiel, R. W. Ziolkowski, and I. M. Besieris, "Spectral analysis of time-limited pulsed Gaussian wavefields," *J. Opt. Soc. Am.*, Vol. A13, 1817–1835, 1996.
73. Sedky, S. M., A. M. Shaarawi, F. M. Taiel, and I. M. Besieris, "On the diffraction length of localized waves generated by dynamic apertures," *J. Opt. Soc. Am.*, Vol. A13, 1719–1727, 1996.
74. Lu, J. Y., M. Fatemi, and J. F. Greenleaf, "Pulsed-echo imaging with X wave," *Acoust. Imag.*, P. Tortoli and L. Masotti, Eds., Vol. 22, 191–196, 1996.
75. Lu, J. Y., "Producing bowtie limited diffraction beams with synthetic array experiment," *IEEE Trans. Ultrason. Ferroelec. Freq. Contr.*, Vol. 42, 893–900, 1996.

76. Hillion, P., "Distortion-free progressing waves," *Europhys. Lett.*, Vol. 33, 7–10, 1996.
77. Hillion, P., "Diffraction of focus wave modes at a perfectly conducting screen," *Opt. Comm.*, Vol. 123, 215–224, 1996.
78. Fagerholm, J., A. T. Friberg, J. Huttunen, D. P. Morgan, and M. M. Salomaa, "Angular-spectrum representation of nondiffracting X waves," *Phys. Rev.*, Vol. E54, 4347–4352, 1996.
79. Sonajalg, H., and P. Saari, "Suppression of temporal spread of ultrashort pulses in dispersive media by Bessel beam generators," *Opt. Lett.*, Vol. 21, 1162–1164, 1996.
80. Shvartburg, A. B., *Time-Domain Optics of Ultrashort Waveforms*, Clarendon Press, Oxford, 1996.
81. Donnelly, R., and D. Power, "The behavior of electromagnetic localized waves at a planar interface," *IEEE Trans. Antennas Propagat.*, Vol. 45, 580–591, 1997.
82. Lu, J. Y., "Designing limited diffraction beams," *IEEE Trans. Ultrason. Ferroelec. Freq. Contr.*, Vol. 44, 181–193, 1997.
83. Friberg, A. T., J. Fagerholm, and M. M. Salomaa, "Space-frequency analysis of nondiffracting pulses," *Opt. Comm.*, Vol. 136, 207–212, 1997.
84. Sonajalg, H., M. Rastep, and P. Saari, "Demonstration of the Bessel-X pulse propagating with strong lateral and longitudinal localization in a dispersive medium," *Opt. Lett.*, Vol. 22, 310–312, 1997.
85. Abdel-Rahman, M., I. M. Besieris, and A. M. Shaarawi, "A comprehensive analysis of propagation of localized waves in collisionless plasma media," *J. Electromagnetic Waves Appl.* (accepted).
86. Shaarawi, A. M., "Comparison of two localized wavefields generated from dynamic apertures," *J. Opt. Soc. Am. A,* Vol. 14, 1804–1816, 1997.
87. Chatzipetros, A. A., A. M. Shaarawi, I. M. Besieris, and M. A. Abdel-Rahman, "Aperture synthesis of time-limited X-waves and analysis of their propagation characteristics," *J. Acoust. Soc. Am.*, (accepted).
88. Overfelt, P. L., "Comment on: On the evanescent fields and the causality of the focus wave modes," *J. Math. Phys.*, Vol. 38, 3391–3395, 1997.
89. MacKinnon, L., *Found. Phys.*, Vol. 8, 157, 1978; *Lett. Nuovo Cim.*, Vol. 31, 37, 1981.
90. Gradshteyn, I. S., and I. M. Ryzhik, *Tables of Integrals, Series and Products*, Adademic Press, New York, 1980.
91. Erdelyi, A., Ed., *Tables of Integral Transforms*, Vol. I, McGraw-Hill, New York, 1954.

92. Devaney, A. J., and G. C. Sherman, "Plane-wave representations for scalar wave fields," *SIAM Rev.,* Vol. 15, 765, 1973.
93. Cornille, P., "An electromagnetic wave approach to matter and radiation," *J. Electromagn. Waves Appl.,* Vol. 8, 1425, 1994.
94. Rodrigues, Jr., W. A., and J.-Y. Lu, "On the existence of undistorted progressive waves (UPWs) of arbitrary speeds $0 < v < \infty$ in nature," *Found. Phys.,* Vol. 27, 435, 1997.